Helsinki University of Technology

Department of Chemical Technology

Laboratory of Physical Chemistry and Electrochemistry

Espoo 2002

ELECTROCHEMISTRY AT ELECTRIFIED SOFT INTERFACES – NOVEL APPROACHES TO OLD PROBLEMS

Peter Liljeroth

TEKNILLINEN KORKEAKOULU
TEKNISKA HÖGSKOLAN
HELSINKI UNIVERSITY OF TECHNOLOGY
TECHNISCHE UNIVERSITÄT HELSINKI
UNIVERSITE DE TECHNOLOGIE D'HELSINKI

ELECTROCHEMISTRY AT ELECTRIFIED SOFT INTERFACES – NOVEL APPROACHES TO OLD PROBLEMS

Peter Liljeroth

Dissertation for the degree of Doctor of Science in Technology to be presented with due permission of the Department of Chemical Technology, for public examination and debate in Komppa Auditorium at Helsinki University of Technology (Espoo, Finland) on the 28th of September, 2002, at 12 noon.

Abstract

This thesis addresses some known difficulties in the field of liquid | liquid electrochemistry by presenting novel means of controlling mass transfer, monolayer-modification of the interface, and probing interfacial reactivity.

A novel rectangular channel flow electrochemical cell suitable for studying charge transfer at liquid | liquid interfaces is presented. The organic phase is immobilised using a gelling agent, while the aqueous phase flows past the interface. This creates an asymmetric diffusion regime, providing diagnostic criteria to determine, for example, the direction of the ion transfer.

One of enduring problems concerning phospholipid adsorption at liquid | liquid interfaces has been the inability to determine and control the exact nature of the adsorbed monomolecular layer. This difficulty is addressed by a combination of the Langmuir-Blodgett technique and the use of an electrochemical cell as a substrate. It is shown that reproducible layers of known surface pressure can be deposited at the interface and that the deposition surface pressure has a great influence on the behaviour of the layer.

The latter part of this thesis concerns the study of reactivity at liquid | liquid interfaces. To this end, the potential of ring-disk ultramicroelectrodes as probes for scanning electrochemical microscopy is investigated both theoretically and experimentally. In particular, the disk-generation/ring-collection mode of operation is considered. The interaction of two species with the substrate under investigation can be followed simultaneously from a single tip current-distance measurement to the substrate. This method is then applied to investigate the partitioning of iodine across a liquid-liquid interface.

A facile method to determine the lipophilicity of potentially unstable charged products of electron transfer reactions is reported. This is achieved by local electrolysis at a Pt coated micropipette and subsequent transfer of the electrogenerated ions across a polarisable liquid | liquid interface supported at the tip of the micropipette. The formal potential of ion transfer can then be used to give a measure of its relative lipophilicity.

Preface

This work was carried out at the Laboratory of Physical Chemistry and Electrochemistry, Helsinki University of Technology, Finland from July 2000 to May 2002 and at the Department of Thermodynamics, University of Valencia, Spain from May 1999 to December 1999.

I would like to thank Prof. Kyösti Kontturi for supervision of work presented herein. In addition, I am indebted to Drs. Bernadette Quinn and Lasse Murtomäki, Prof. José Manzanares and M.Sc. Christoffer Johans for useful discussions throughout this time. I am also grateful to other co-authors M.Sc. Annika Mälkiä and Drs. Annu Kontturi, Vincent Cunnane, and Chris Slevin for fruitful collaboration.

Espoo, 4th September 2002

Peter Liljeroth

Contents

List of Publications

I. Peter Liljeroth, Christoffer Johans, Kyösti Kontturi, José A. Manzanares, Channel Flow at an Immobilised Liquid | Liquid Interface, *J. Electroanal. Chem.* **483** (2000) 37–46.

II. Peter Liljeroth, Annika Mälkiä, Vincent J. Cunnane, Anna-Kaisa Kontturi, Kyösti Kontturi, Langmuir-Blodgett Monolayers at a Liquid | Liquid Interface, *Langmuir* **16** (2000) 6667–6673.

III. Peter Liljeroth, Christoffer Johans, Christopher J. Slevin, Bernadette M. Quinn, Kyösti Kontturi, Micro Ring-Disk Electrode Probes for Scanning Electrochemical Microscopy, *Electrochem. Commun.* **4** (2002) 67–71.

IV. Peter Liljeroth, Christoffer Johans, Christopher J. Slevin, Bernadette M. Quinn, Kyösti Kontturi, Disk-Generation / Ring-Collection Scanning Electrochemical Microscopy; Theory and Application, *Anal. Chem.* **74** (2002) 1972-1978.

V. Peter Liljeroth, Bernadette M. Quinn, Kyösti Kontturi, Lipophilicity of Ions Electrogenerated at a Pt Coated Micropipette Supported Liquid-Liquid Interface, *Electrochem. Commun.* **4** (2002) 255–259.

This thesis also includes the following unpublished work:

A. Partitioning studies with RD-SECM

Statement on the Author's Role

In the case of papers I, III and IV, Peter Liljeroth has done almost all experimental work. In paper II, the experimental work was performed jointly by Liljeroth and Mälkiä and in paper V, jointly by Liljeroth and Quinn. Liljeroth has taken an active part in planning of the experimental work, interpretation of results, and was the principal author of the papers included here. The theoretical work included in the papers has been done by Liljeroth.

In addition to these papers, the thesis contains unpublished results on iodine partitioning studied by scanning electrochemical microscopy.

Espoo, 4th September 2002

Kyösti Kontturi

Professor

1 Introduction

Electrochemistry at the interface between two immiscible electrolyte solutions (ITIES) is a rather new field in electrochemistry; while the first studies were done at the turn of the century, it is only since the early 1980s that this field has seen real progression.[1–9] In a traditional electrochemical experiment at a metal electrode, the potential of the working electrode is controlled with respect to a reference electrode. This applied potential can then drive electron transfer which occurs at the electrode-solution boundary. In an ITIES experiment, a potential difference is applied between two reference electrodes located in the opposing phases, *i.e.* the "working" electrode is, in fact, the interface. The potential difference can act as a driving force for charge transfer reactions that can be divided into three categories: ion transfer (IT), electron transfer (ET), and facilitated ion transfer (FIT). The polarisability of the interface depends on the choice of electrolytes in both phases: it can approach ideally non-polarisable conditions if the interfacial potential difference is fixed by the presence of a common ion. On the other hand, if only very hydrophilic and hydrophobic electrolytes are used, the interface can be termed ideally polarisable, *i.e.* there exists a potential region, the so-called potential window, where little or no faradaic current flows. An ion transfer reaction

$$X^z(\text{aq}) \rightleftarrows X^z(\text{org}) \tag{1}$$

can be characterised by a quantity called the standard transfer potential, $\Delta_\text{o}^\text{w}\phi^0$, that gives a measure of the hydrophilicity/hydrophobicity of the ion. It is given for species i by the difference of the solvation energies in the respective phases

$$\Delta_\text{o}^\text{w}\phi_i^0 = \frac{\Delta G_{i,\text{tr.}}^{\text{w}\to\text{o}}}{z_i F} = \frac{\mu_i^{0,\text{o}} - \mu_i^{0,\text{w}}}{z_i F} \tag{2}$$

where $\Delta G_{i,\text{tr.}}^{\text{w}\to\text{o}}$ is the Gibbs free energy of transfer of species i, z_i the charge of ion i, F the Faraday constant, $\mu_i^{0,\text{o}}$ and $\mu_i^{0,\text{w}}$ are the standard chemical potentials of ion i in the organic and aqueous phases, respectively. This standard transfer potential has no relation to the standard redox potential of the ion, E_i^0. The interfacial potential difference can be fixed by having a common ion in both phases, that is, electrochemical reactions can be driven without external potential control. The

second mode of charge transfer, heterogeneous electron transfer, occurs between aqueous (1) and organic (2) redox couples

$$\mathrm{Red_1(aq) + Ox_2(org) \rightleftarrows Ox_1(aq) + Red_2(org)} \qquad (3)$$
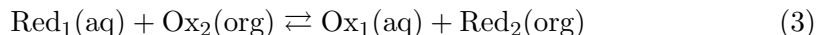
Facilitated ion transfer is a special case of ion transfer, which can be thought of as ion transfer followed by a complexation reaction. However, the complexation reaction may only occur interfacially

$$\mathrm{X^z(aq) + L(org) \rightleftarrows X^zL(org)} \qquad (4)$$
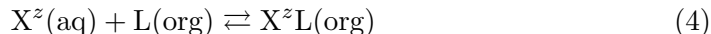
where L is a ligand capable of complexing the ion X^z. The mechanism of facilitation is to lower the solvation energy in the receptor phase.

In addition to instrumental differences and the possibility of charge transfer involving ions, there are other notable differences between liquid | liquid and more traditional metal electrode electrochemistry: a liquid | liquid interface is dynamic in nature, the interaction between possible surface active molecules and the interface is significantly weaker than at metal electrodes, and the interface is free from any preferential sites, such as the kink sites on metal electrode surfaces. These properties make the liquid | liquid interface a very attractive choice as a substrate for monolayer studies or nucleation experiments.[10–12]

Similarly to electrochemistry at metal electrodes, making the polarisable interface smaller is advantageous, *i.e.* bringing the characteristic dimension down to 50 μm or less. At ITIES, this has been achieved by two alternative strategies, either by supporting the interface at a tip of a micropipette[13] or at a microhole formed by photoablation of a thin polymer film.[14, 15]

Electrochemistry at liquid | liquid interfaces constitutes a fascinating research field with a multitude of applications, such as electroanalysis,[16–20] biomembrane mimetics,[21–25] two-phase catalysis or synthesis,[26–29] solar energy conversion[30, 31] and lipophilicity studies and pharmacokinetics.[32–39] In addition, properties of these soft interfaces are of interest from a purely fundamental point of view. The level of current interest is mirrored in the number of recent reviews and books concerning electrochemistry at liquid | liquid interfaces.[40–45]

There are some major challenges in this field. Refined theoretical and experi-

mental tools are needed to elucidate the interfacial structure on a molecular level. Experimentally, second harmonic (SHG)[46–51] and sum frequency (SFG)[52–58] generation have only recently reached sufficient sensitivity to probe bare liquid-liquid interfaces, while neutron[59] and X-ray[60–62] reflection techniques have been used sparingly. Very recently, quasi-elastic light scattering (QELS) was used to probe the interfacial structure.[63–67] On the theoretical side, molecular dynamics (MD) simulations continue to yield detailed structural information, however, the results are somewhat dependent on the potential function chosen.[68, 69] Furthermore, simulation of the electrochemical double-layer in atomistic detail is still beyond the reach of available computer power. Another challenge is to develop experimental techniques that are capable of probing spontaneous reactions, such as partitioning or coupled charge transfer processes, and complicated reaction mechanisms at interfaces. Important developments in microelectrochemical techniques are making such studies possible.[70–73] Finally, a means to control the assembly molecular layers is necessary to create structurally modified interfaces that could then be used in, for example, selective catalysis, electroanalysis, as improved biomimetic systems, or as templates for other mesoscale structures.

The publications in this thesis make an attempt to address some of the aforementioned issues. Publ. I presents the use of channel flow geometry to control the hydrodynamics at a water | immobilised organic solvent interface. Publ. II introduces a novel combination of the Langmuir-Blodgett (LB) technique where an electrochemical cell is used as a substrate to deposit monomolecular layers at a liquid | liquid interface. Publs. III and IV show how ring-disk (RD) ultramicroelectrodes (UMEs) can be used as probes in scanning electrochemical microscopy (SECM) to study spontaneous reactions at interfaces. Finally, Publ. V offers a new solution to probing the interfacial reactivity of electrogenerated, possibly unstable, species.

More details on each of the publications will be given in the following sections that review some of the relevant recent developments in this area. In addition, previously unpublished simulations on partitioning studies using disk-generation/ring-collection (DG/RC) RD-SECM are presented.

2 Hydrodynamic Methods at ITIES

Prerequisite to any attempt to accurately model an electrochemical experiment is control of the mass transport in the system. This statement is valid whether the experiment in question is conducted for electroanalytical purposes, to obtain kinetic parameters or to elucidate complex reaction mechanisms. At metal electrodes, several hydrodynamic methods have been used for this purpose, such as dropping mercury, rotating disk, channel flow, wall-jet, radial flow microring electrodes, hydrodynamic ultramicroelectrodes, and modulated hydrodynamic electrodes.[74–85] While all of these methods allow accurate modelling of the convective diffusion, they differ in terms of the accessible rates of mass transfer, on whether the electrode is uniformly accessible and the interface periodically renewed. All of these aspects need to be considered in choosing an appropriate technique for a particular purpose. With the exception of hydrodynamic microelectrodes or hydrodynamic modulation voltammetry, all of these methods have also been used in liquid | liquid electrochemistry.

Some of the first liquid | liquid experiments were done using a electrolyte dropping electrode (EDE)[86–88] which is essentially a liquid | liquid analog of the dropping mercury electrode. In this technique, the interface is continually renewed and thus possible problems with interfacial blocking by reactants, products, or impurities are minimised. EDE has been applied to the study of ion transfer, mainly focusing on the electroanalytical aspects based on either ion or facilitated ion transfer. These efforts have been reviewed in the literature.[89] The charging current associated with the constantly changing interfacial area can be used to deduce the interfacial capacitance and tension. Baars *et al.* introduced a fast miniaturisation of EDE[90] to study the water | nitrobenzene system in the presence of base electrolytes only. EDE has been developed further in what is termed "microelectrochemical measurements at expanding droplets" (MEMED). This technique incorporates a microelectrode to directly probe the concentration profiles of reacting species at an expanding liquid | liquid interface, making it possible to study interfacial fluxes directly.[72,73,91,92] MEMED will be further considered in the section 4.

The liquid | liquid analogy to the rotating disk electrode is the "rotating diffusion cell" (RDC), first introduced by Albery *et al.*[93] In RDC, the interface is

supported in a thin porous membrane (either hydrophilic or hydrophobic) between the inner and outer compartments of the cell. The membrane is rotated in the solution and the hydrodynamic boundary layers of a rotating disk are established on both sides of the membrane. A number of different configurations are possible, with the most common one involving aqueous solutions in both the inner and outer compartments, with the organic phase impregnated within the membrane. This was also the setup used to study ion (tetrabutylammonium) transfer at a polarised water | nitrophenyl octyl ether (NPOE) interface.[94]

A wall-jet setup was introduced in the liquid-liquid context by Mareček *et al.*[95] Poly(vinylchloride) supported nitrobenzene was used as the organic phase and the transfer of acetylcholine by differential pulse voltammetry (DPV) was studied . Hundhammer and Wilke used an analogous setup to conduct electroanalytical measurements of perchlorate, thiocyanate, iodide, nitrate, bromide, and chloride ions at a hydrophobic membrane stabilised water | nitrobenzene interface.[96] In a similar study, Wilke *et al.* demonstrated simultaneous detection of nitrate and chloride in a wall-jet configuration.[97]

A flow-through cell, basically equivalent to the channel flow cell (CFC), has been used in liquid | liquid electrochemistry by several authors.[18,19,98–100] These authors have employed flow cells for electroanalytical purposes and, subsequently, no theory for the hydrodynamics or the mass transport in the channel has been given. Wang and Ji employed nitrobenzene immobilised with PVC as the organic phase while the aqueous phase was the mobile phase in this flow-through construction.[98] They demonstrated amperometric analysis of choline, acetylcholine, tetramethylammonium, tetrabutylammonium, cesium, perchlorate, periodate, and perrhenate. Sawada *et al.* also used a macroscopic interface in a flow cell to analyse lithium ion in artificial serum.[19] An interesting development was achieved Girault and co-workers: initially, the use of a micro interface in a flow system[18,100] to detect various cations and salts and then a complete miniaturisation consisting of a photo-ablated microchannel and a microhole supported liquid | liquid interface as a detector.[99] This microdevice was used in a polymer capillary electrophoresis system with an integrated electrochemical detector.

A quite different application of a channel flow geometry at liquid-liquid interfaces has been introduced by Fisher and co-workers:[101,102] Two separate solvent
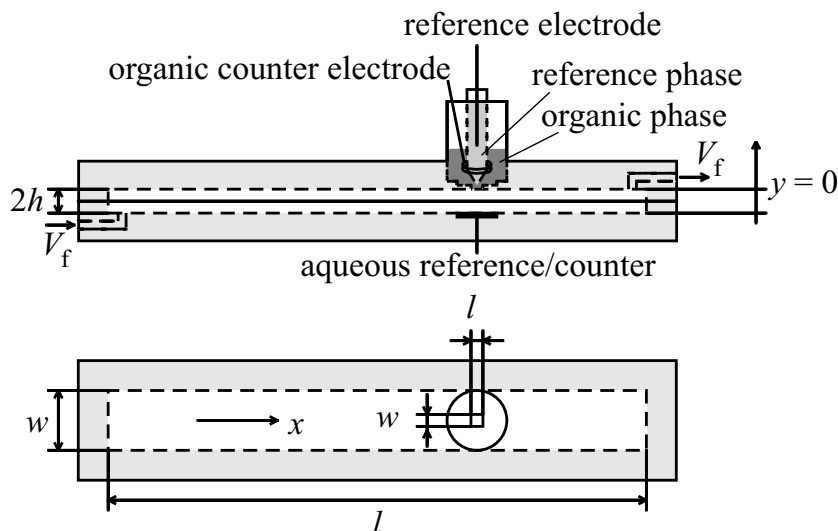
Figure 1: A schematic of the channel-flow cell used in Publ. I. The organic phase is immobilised using PVC, while the aqueous phase flows parallel to the interface.

streams enter a membrane separated reaction chamber where reagents in the solvents may then partition between the phases. An inert porous polymer membrane at the interface is used to stabilise the flow fields and impose well-defined and controllable mass transport within the cell. The flux of material through the interface is monitored voltammetrically at an electrode placed in either phase. This construction was used in a preliminary study to measure iodine transfer between 1,2-dichloroethane (DCE) and water.[101]

The history of the hydrodynamic methods at ITIES has also recently been reviewed.[103] The application of hydrodynamic systems at liquid | liquid interfaces has mainly concentrated on electroanalytical applications, and more sophisticated aspects such as increased discrimination towards different reaction mechanisms caused by non-uniform accessibility of the interface, have not been considered. Furthermore, rigorous modelling of the mass transport has not been presented, apart from the microelectrochemical measurements at expanding droplets and the work by Fisher *et al.* on channel flow. However, these two approaches differ from conventional liquid | liquid electrochemistry in that current through the liquid-liquid interface is not measured and the interface is not externally polarised.

Publ. I presents the application of a well-defined channel flow electrochemical cell to the study of an externally polarised liquid | liquid interface. The organic

14

phase (NPOE) was immobilised by the use of a gelling agent (PVC), while the aqueous phase flows parallel to the interface, see Fig. 1. A simplified theoretical approach based on the Singh-Dutt approximation (the use of average concentration values along the flow)[104, 105] was presented and this simplification was validated by simulations of the full, two-dimensional convective diffusion equation. Cyclic voltammetry was used to investigate tetraethylammonium cation (TEA$^+$) transfer across the liquid | liquid interface as a function of the sweep and volumetric flow rate. As expected, the shape of the cyclic voltammograms was asymmetric providing clear diagnostic criteria for the direction of ion transfer. This asymmetry is due to the difference in diffusion geometries in each phases: convective (forced) diffusion in the aqueous phase and linear diffusion in the immobilised organic phase. The absence of steady-state due to linear diffusion in the organic phase was noted to cause a shift in the observed half-wave potential with the dimensionless sweep rate (combination of the sweep rate and the volumetric flow-rate). Experimental half-wave potential was in good correspondence with theoretical predictions. This well-defined hydrodynamic liquid | liquid interface could be used in future mechanistic studies to probe liquid-liquid reactivity, perhaps in combination with a detector electrode or a UV-detection located immediately downstream from the interface.

3 Modified Liquid | Liquid Interfaces

Early studies at monolayer-modified liquid | liquid interfaces focused on the effect of adsorbed phospholipid monolayer on the interfacial capacitance / tension[21, 106–110] and charge transfer.[111–116] The monolayer in these studies was formed by a self-assembly process leading to rather expanded monolayers. The interfacial tension is naturally greatly reduced by the addition of a lipid monolayer, and the adsorption is potential dependent. At not too positive potentials ($\Delta_o^w \phi < 0.1$V), the interfacial tension is low and constant, however, at the positive end of the potential window($\Delta_o^w \phi > 0.15$V), the interfacial tension starts to abruptly increase.[21, 106, 109] This has been attributed to either a surface reorientation of the phospholipid layer accompanied by neutralization of the phosphate group in the polar head group[21, 106] or desorption.[109] Upon adsorption of a phosphatidylcholine monolayer at the interface, the potential of zero charge also shifted to a more negative potential indicating specific adsorption of aqueous cations to the lipid head group.[110]

Initial studies on ion transfer across adsorbed monolayers by cyclic voltammetry usually found that the monolayer acts as an additional energy barrier to ion transfer.[111, 112] However, subsequent investigations using more sophisticated electrochemical techniques such that ac voltammetry or impedance spectroscopy did not detect such strong retardation,[113, 114] and an enhancement of the rate of ion transfer has also been reported.[113, 115]

Electron transfer through phospholipid layers initially attracted little attention, most likely due to various experimental difficulties associated with electron transfer studies at these interfaces.[117] An early study by Cheng and Schiffrin considered ET between aqueous phase hexacyanoferrate and a variety of organic phase redox couples (tetracyanoquinodimethane (TCNQ), bis(pyridine)-tetraphenylporphyrinato-ruthenium (Ru(TPP)(py)$_2$) and lutetium bisphthalocyanine (Lu(PC)$_2$)) at the water | DCE interface in the presence of adsorbed phospholipid.[26] The presence of a monolayer inhibited electron transfer reaction to an increasing extent in the following order: TCNQ, Ru(TPP)(py)$_2$, Lu(PC)$_2$. The central result of the study was the observed mediation of electron transfer by TCNQ in a redox electrocatalytic cycle for the reaction between Ru(TPP)(py)$_2$ and aqueous hexacyanoferrate. Recently, the advent of advanced microelectrochemical methods,

such as SECM and MEMED, have made this area more experimentally tractable and there has been a number of papers treating the effect of an adsorbed monolayer on IT, ET or molecular transport kinetics.[91, 118–123] Tsionsky *et al.* probed the rate of electron transfer as a function of driving force and distance between redox centers with SECM. The adsorption of phospholipids at the interface resulted in a decrease in the rate of interfacial ET between the aqueous redox species and the oxidised form of zinc porphyrin in benzene. The dependence of the logarithm of the rate constant on the reaction driving force was linear at low overpotentials, while inverted Marcus region behaviour was observed at very high driving force.[119] Another interesting study was conducted by Delville *et al.* who studied the effect of chain saturation on the rate of electron transfer through monolayers of saturated dipalmitoyl phosphatidylcholine (DPPC) and polyconjugated 2(3-(diphenylhexatrienyl)propanoyl)-1-hexadecanoyl-*sn*-glycero-3-phosphatidylcholine phospholipids. Comparison of the ET rates showed that the addition of phospholipids with conjugated hydrocarbon chains increases the ET rate by at least a factor of two compared to films with only saturated hydrocarbon chains.[118] In addition, a sharp decrease in the ET rate with decreasing temperature was observed. This was attributed to a phase transition of the hydrocarbon chains of the lipid molecules. Using MEMED, Zhang *et al.* investigated the effect of the nonionic surfactant Triton X-100 on the ET reaction between TCNQ and $Fe(CN)_6^{4-}$ and found that the effect of surfactant can be accounted for by the free area model, *i.e.* the electron transfer rate is proportional to $1 - \theta$,[91] where θ is the surface coverage. In another study, Zhang and Unwin studied $IrCl_6^{2-}$ ion transfer across a water | DCE interface both in the presence and absence of phospholipid monolayers using SECM and MEMED.[123] The phospholipid was found to significantly diminish the rate of IT, with the retardation effect dependent on the interfacial phospholipid concentration.

A drawback associated with self-assembled monolayers is that there is an uncertainty as to the exact state of the layer due to the inability to control the surface pressure. It would therefore be highly desirable to control the state of the monolayer by external means. Two conceivable methods would be either to control the surface pressure *in situ* or to transfer a monolayer already in the desired state to the interface. The former case has been realised in the combination of

the Langmuir technique with electrochemical control over the interfacial potential difference.[124–126] Electrochemically, however, this design suffers from the resulting large interfacial area and invalidates the use of ac voltammetry or impedance spectroscopy. These techniques are required if quantitative information on interfacial capacitance and membrane activity of various probe ions is to be extracted. Monolayer loss to the bulk organic phase and large volumes of toxic organic solvent present additional drawbacks.

Despite the shortcomings of an adsorbed monolayer, it is an adequate substrate for some studies, such as the study of hydrolysis of the monolayer induced by enzymes[23,24] or mediated electron transfer.[127] Kondo *et al.* studied enzymatic hydrolysis of a phosphatidylcholine monolayer by phospholipase D at the water | nitrobenzene interface by following the change in interfacial capacitance. The rate of the hydrolysis was markedly dependent on the potential drop across the interface: at negative potentials, no hydrolysis was observed, whereas at positive potentials, the hydrolysis proceeded rapidly.[23] In a related study, the relative effectiveness of different phospholipases was assessed.[24] Georganopoulou *et al.* examined the reactivity of glucose oxidase adsorbed at the dichloroethane/water interface by probing heterogeneous electron transfer.[127]

The majority of studies at modified liquid | liquid interfaces have considered adsorption of lipids either from a biomimetic[10,106] or fundamental point of view.[119] It is, however, also possible to modify the interface with a porous mask, and toward this end, both zeolite[128,129] or polyethylene terephthalate[130,131] membranes have been proposed. Dryfe and Holmes reported modification of the water | DCE interface with a zeolite layer: application of a potential difference across the modified interface allowed the selective transfer of ionic species on the basis of the dimensions of the transferring ion with respect to those of the zeolite pores.[128] This methodology was subsequently used in electroanalysis.[129] In another study, Dryfe and Kralj showed that "track-etched" polyester membranes can be used to generate a nanoscale array. The electrochemical response is consistent with the location of the ITIES within the pores of the membrane material, *i.e.* ensembles of micro-ITIES are generated by this procedure.[130,131] The polymer film modified interface has very recently been used as a template in nucleation studies.[132]

As an extreme example of modified liquid | liquid interfaces, Corn *et al.* re-
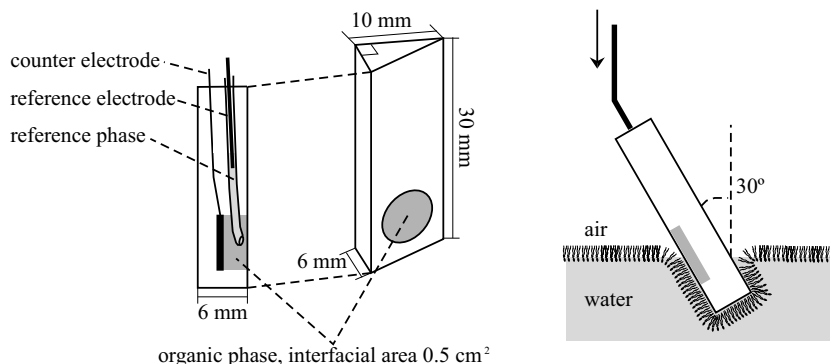
Figure 2: Langmuir-Blodgett deposition procedure for producing monolayers at liquid | liquid interfaces.

cently devised a method whereby a liquid-liquid interface is created by an ultra-thin hydrophilic polypeptide film at a chemically modified gold surface in contact with DCE electrolyte solution. The hydrophilic films were prepared by sequential layer by layer electrostatic adsorption of polypeptides, poly-L-lysine and poly-L-glutamic acid, onto gold thin films derivatised with an ω-carboxylic acid function-alised alkanethiol monolayer. The polypeptide film thickness could be varied from 5 to 30nm, and it was possible to incorporate ionic electroactive species such as hexacyanoferrate into the film.[133, 134]

Publ. II considers another possibility of applying a monolayer at a liquid | liquid interface in a controlled manner, that is, transferring a monolayer of distearoyl phosphatidylcholine (DSPC) in a defined state onto a liquid | liquid interface by the use of the Langmuir-Blodgett technique. This technique has been used exten-sively to produce mono- and multilayer films on solid substrates and involves first assembling a monolayer at the air-water interface and then transferring it onto a substrate (see Fig. 2). The present study is unique in the choice of the substrate. Instead of using a conventional solid substrate, for example a glass slide, an elec-trochemical cell is dipped through the monolayer at the air-water interface. As illustrated in Fig. 2, the organic phase is immobilised by the use of a gelling agent (PVC) and the body of the cell is made of hydrophobic poly(tetrafluoroethene) (PTFE, Teflon). Upon immersion into the subphase, the entire cell, including the interface, is covered by the monolayer. The monolayer was characterised by four-electrode cyclic voltammetry, which yielded both capacitance data and in-

19

formation on ion permeability of the monolayer. The deposition surface pressure had a great influence on the behavior of the monolayer. At the lower deposition pressures, the capacitance was low at negative potentials ($\Delta_o^w\phi < 0$V), but approached that of bare interface at positive potentials ($\Delta_o^w\phi > 0.05$V). At higher deposition pressures (> 50mN/m), the capacitance decreased significantly and was approximately constant. In addition, in the presence of adsorbed lipid monolayer, the electrocapillary curve shifted negative. These observations were interpreted using a simple electrostatic model, in which aqueous cation binding to the zwitterionic phospholipid head group is responsible for the shift in the minimum of the capacitance curve, while the decreased dielectric constant and organic electrolyte concentration in the hydrocarbon domain of the monolayer result in lower values of interfacial capacitance. Subsequently, this LB-deposition technique was used to probe the membrane activity of ionisable drugs both at pure and mixed phospholipid monolayer-modified interfaces.[10,135]

4 Probing Interfacial Reactivity

One of the advantages of electrochemistry is that the current gives a direct measure of the rate of net charge transfer across the interface. However, there are several phenomena that do not induce current flow as they do not involve net charge transfer. The study of these processes is not straightforward and it has mainly been approached either by *in situ* spectroscopic techniques to measure the concentration of the species of interest, or by taking samples from the system followed by *ex situ* analysis. Recently, electrochemical alternatives for probing such processes have been developed: generation/collection experiments with double potential step chronoamperometry (DPSC) using SECM[70, 71, 123] and MEMED.[72, 73, 91, 92]

The scanning electrochemical microscope is a scanned probe microscope (SPM) related to the familiar scanning tunneling (STM) and atomic force microscopes (AFM). All SPMs operate by scanning or "rastering" a small probe tip over the surface to be imaged. In SECM, imaging occurs in an electrolyte solution with an electrochemically active tip. In most cases, the SECM tip is an ultramicroelectrode and the tip signal is the faradaic current response from electrolysis of solution species. Some SECM experiments use an ion-selective electrode (ISE) as the tip. Two features distinguish SECM from related methods such as electrochemical STM or AFM: the chemical sensitivity of the SECM tip and the use of solution phase ions or molecules as the imaging signal. SECM operation principles and application have been extensively reviewed.[136–144]

The concept of DPSC-SECM is to generate a reactant in an initial potential step at a tip UME positioned close to a target interface. The electrogenerated species diffuses from the tip to the interface, where it may be involved in a chemical process. The reactant is subsequently collected by electrolysis in a second potential step, and the resulting current-time curve provides information on the nature of the interaction between the initial tip-generated species and the interface. If the species is consumed in an irreversible interfacial process, the current flow during the second potential step is less than when the interface is inert with respect to the species of interest. This mode of SECM has been used to study the partitioning of Br_2 into DCE,[70] transfer of ferricinium,[71] and the effect of a phospholipid monolayer on the transfer of iridium hexachloride.[123] DPSC-SECM studies generally require the use of high concentrations of the redox mediator to diminish the effects of double-layer

charging and other non-idealities on the amperometric response to access the short time-scales that are needed to gain full advantage of this transient based technique. In addition, 10ms potential steps typically employed set stringent requirements in terms of the electrochemical instrumentation.

MEMED involves establishing the interface by forming drops of one liquid from a capillary submerged in the second liquid, in a manner similar to the dropping mercury electrode. The feeder solution flows into the receptor solution at a constant rate such that drops form, grow and detach periodically in a well-defined way, and the interface is constantly refreshed. The interfacial reaction is probed by an UME positioned in the receptor phase at a fixed distance directly below the capillary, which measures local concentration changes as drops growing from the capillary approach it until contact. The electrode thus directly probes the concentration gradient extending from the drop surface into the receptor phase under the conditions of convective-diffusion at an expanding drop. Initial MEMED studies investigated the hydrolysis of triphenylmethylammonium chloride at the water-DCE interface.[72] Subsequently, both bromine partitioning and electron transfer between aqueous phase $IrCl_6^{2-}$ and organic phase ferrocene were investigated.[73,92] Very recently, this technique was used to investigate the effect of Triton X-100 (a nonionic surfactant) on ET kinetics[91] and the mechanism of 4-methylanisole oxidation by Ce(IV).[145]

Another hydrodynamic method capable of probing reactions that involve no overall net charge transfer was proposed by Fulian *et al.*[101] The authors outlined the development of a new hydrodynamic device to investigate probing reactions which occur when ions or uncharged molecules are transferred between an organic and an aqueous solvent, as outlined in section 2. The species of interest, in this case iodine, was detected voltammetrically in the aqueous phase.

Publ. III present an alternative to the generation-collection experiments with DPSC-SECM by introducing a micro ring-disk electrode as a SECM probe. The manufacture of carbon ring-disk ultramicroelectrodes (RD-UME) by chemical vapour deposition (CVD) and preparation of ring UME SECM tips by vapour deposition of a gold film onto a pulled optical fibre followed by insulation by electrophoretic paint have been reported previously.[146,147] Publ. III is the first report, however, where a RD-UME was used as a SECM probe. The RD tips were pre-
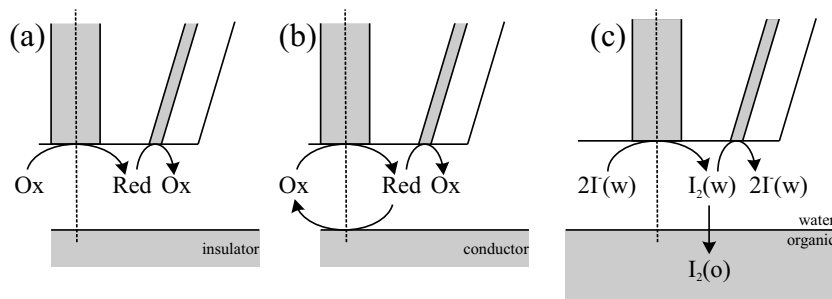
Figure 3: Schematic presentation of the different possible processes in a RD-SECM experiment: (a) approach to an insulating substrate, (b) approach to a conducting substrate, and (c) study of iodine partitioning across a liquid-liquid interface.

pared by simply sputtering a gold film onto a normal disk SECM tip, applying an insulating varnish and subsequent polishing to expose the ring-disk electrode. The measurements can be carried out under steady-state conditions which overcomes the difficulties associated with double-layer charging or time resolution of the instrument. In the proposed disk-generation/ring-collection (DG/RC) mode of operation, a redox mediator reacts under diffusion controlled conditions at the disk and is regenerated at the ring electrode, as can be seen in Fig. 3. For the collector ring electrode, as the tip approaches an insulator (Fig. 3 (a)), diffusion of Red away from the disk is blocked by the substrate and initially, the ring current increases. However, at closer distances, the ring current decreases as the amount of disk-generated Ox is reduced. In contrast, for an approach to a conducting substrate (Fig. 3 (b)), the concentration changes due to the reaction at the disk are localised in the disk-substrate gap and, thus the collection current at the ring decreases to zero, as positive feedback at the disk increases.

Conceptually, this mode of operation resembles the DPSC-SECM, wherein a precursor is electrolysed at the tip during the forward potential step and then, subsequently, the electrode-generated species is collected during a reverse potential step. However, a distinct advantage of RD-SECM in comparison with the DPSC-SECM is that low concentrations of the electroactive species can be employed as the measurements are carried out in steady-state and double-layer charging current is absent.

Very recently, Ulheil *et al.* proposed ultramicroheptodes as SECM tips wherein the "ring" is formed by six ultramicroelectrodes located on a circle around the mid-
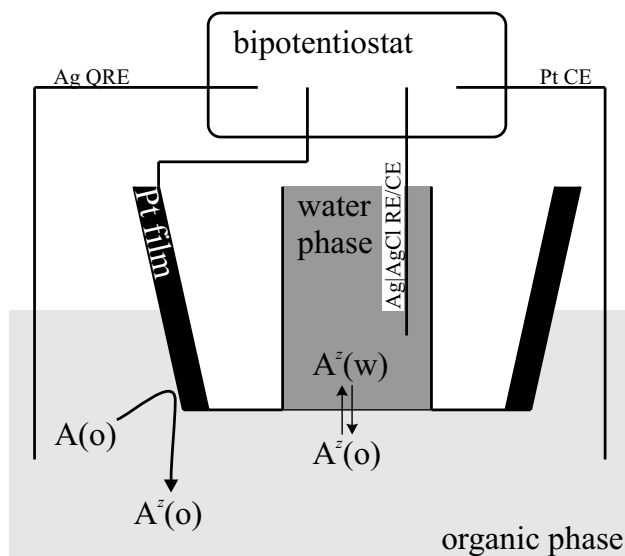
Figure 4: Schematic presentation of the assembly used in Publ. V.

dle disk electrode.[148] They presented experimental data for both disk-generation / "ring"-collection and "ring"-generation / disk-collection experiments, however, no theory was presented for the generation-collection experiments.

Theoretical treatment of DG/RC mode of SECM operation is outlined in Publ. IV and the method is applied to study iodine partitioning across water | 1,6-dichlorohexane (DCHx). As Fig. 3 (c) schematically shows, iodide is oxidised at the disk electrode to form iodine. Iodine readily partitions across the liquid-liquid interface into the DCHx phase, and this change (compared to an insulating substrate) is detected at the ring where iodine is collected. The partitioning process is analysed theoretically in more detail in the next section.

Publ. V presents another method of studying interfacial reactivity of electrogenerated species. This was achieved by *in situ* localised electrolysis of the reactant in the vicinity of a polarised liquid | liquid interface supported at the tip of a micropipette (see Fig. 4). The lipophilicity of the generated species is then probed by measuring its transfer potential across a polarised liquid | liquid interface. For example, the transfer of coat electrode generated ferricinium (Fc^+) ion according to the reaction $Fc \rightarrow Fc^+ + e^-$ can be visualised by the appearance of an additional wave in the voltammetric response of the liquid | liquid interface, as illustrated in Fig. 2 of Publ. V.

The formal potential of ion transfer can then be used to give a measure of its relative hydrophilicity/hydrophobicity. The organic phase redox reactants considered for ET studies are generally neutral species whereby the charged species is generated by the heterogeneous ET reaction from an aqueous phase reactant. Such organic charged products are not generally commercially available and thus their lipophilicity has not been readily accessible. It has been probed indirectly by such techniques as DPSC-SECM.[71] The charged species can be also generated by *ex situ* bulk electrolysis of the neutral species.[149] However, this is problematic in highly resistive organic solvents such as 1,2-dichloroethane without the addition of large quantities of supporting electrolyte. Chemical oxidation/reduction methods[150] are also possible, though lability and purification of the resulting species have to be considered.

In contrast to the previous examples, the present method involves an externally polarised liquid | liquid interface in combination with a metal | electrolyte interface. The technique is demonstrated for some of the most commonly studied organic redox species; decamethylferrocene (DcFc), dimethylferrocene (DmFc), ferrocene (Fc), ferrocene methanol (FcMeOH), tetrathiafulvalene (TTF) and tetracyanoquinodimethane (TCNQ). In addition to measuring the standard potentials of transfer of the ionic species, the effect of adding a salting-out agent is investigated. All the ions studied here, with the exception of $TCNQ^{\cdot-}$, could be classified as relatively hydrophilic as they transfer readily within the available potential window. In most studies concerning heterogeneous ET at ITIES, the possibility of coupled ion transfer has not been considered. In light of this study, coupled charge transfer should not be discounted *a priori*.
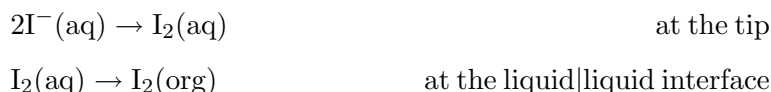
In conclusion, the Pt coated micropipette assembly is a facile method, requires only very small volumes ($< 100\mu l$) of both phases, and enables a lipophilicity study of potentially unstable charged products of electron transfer reactions.

5 Partitioning Studies with RD-SECM

5.1 Introduction

Due to the cylindrical geometry of the SECM microelectrode probe, the diffusion problem does not usually warrant an analytical solution or, at least, it is very complicated. Therefore, a number of different numerical methods has been used to approach SECM related problems. The first SECM simulations used the finite element method (FEM) but this method has been used relatively little since.[151] An offshoot of FEM, called the boundary element method (BEM), has also been used to simulate SECM, especially in connection with complex electrode geometries (hemi-spherical or conical electrodes).[152, 153] The body of SECM simulations have been produced using the alternating direction implicit (ADI) method, which is also the method of choice in the simulations presented here. ADI simulations have been used to look at conventional SECM in the absence and presence of homogeneous chemical reactions,[154–160] SECM in two-phase systems[70, 71, 161–163] and lateral diffusion phenomena in Langmuir monolayers.[164–166] Some simulations have used miscellaneous techniques, such as the Krylov integrator algorithm.[156, 167]

This section presents numerical simulations for DG/RC-SECM experiments for the case where the electrogenerated species, in this case iodine, can irreversibly transfer across the target interface:

$$2\text{I}^-(\text{aq}) \rightarrow \text{I}_2(\text{aq}) \qquad\qquad \text{at the tip}$$

$$\text{I}_2(\text{aq}) \rightarrow \text{I}_2(\text{org}) \qquad\qquad \text{at the liquid|liquid interface}$$

These calculations complement the ones included in Publs. III and IV and in addition, present an application of the finite difference method introduced by Gavaghan[168] for SECM experiments. First, the method used is tested by comparison with known analytical approximations to disk and ring electrodes situated in the bulk of the solution. Secondly, conventional SECM approach curves to both insulating and conducting substrates are simulated. Galceran *et al.*[169] have derived an analytical solution for these cases and thus present an excellent test for the accuracy of the present numerical solution. As a final test, the results for RD-SECM simulations are compared with FEM calculations with an adaptively refined grid.
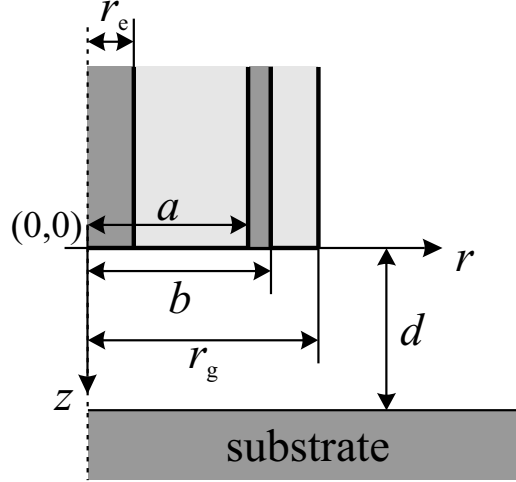
Figure 5: The simulation domain with relevant symbols

Finally, simulation results for different rate constants of the irreversible transfer step are presented.

5.2 Theory

5.2.1 Formulation of the diffusion problem

The diffusion equation for species α in the cylindrical symmetry is

$$\frac{\partial c_\alpha}{\partial t} = D_\alpha \left(\frac{\partial^2 c_\alpha}{\partial r^2} + \frac{1}{r}\frac{\partial c_\alpha}{\partial r} + \frac{\partial^2 c_\alpha}{\partial z^2} \right) \tag{5}$$

This can be written in dimensionless form

$$\frac{\partial C_\alpha}{\partial \tau} = \xi_\alpha \left(\frac{\partial^2 C_\alpha}{\partial R^2} + \frac{1}{R}\frac{\partial C_\alpha}{\partial R} + \frac{\partial^2 C_\alpha}{\partial Z^2} \right) \tag{6}$$

where $C_\alpha = c_\alpha/c^{\mathrm{b}}$, $\tau = Dt/r_{\mathrm{e}}^2$, $\xi_\alpha = D_\alpha/D$, $R = r/r_{\mathrm{e}}$, and $Z = z/r_{\mathrm{e}}$.

In a disk-generation/ring-collection experiment, the species initially present, Ox, is reduced at a diffusion controlled rate at the disk and regenerated at the ring electrode. The electrode reaction is assumed to be a simple n-electron transfer

$$\mathrm{Ox} + n\mathrm{e}^- \rightleftarrows \mathrm{Red} \tag{7}$$

27

The initial conditions are

$$C_{\mathrm{Ox}}(R, Z, \tau = 0) = 1 \tag{8a}$$

$$C_{\mathrm{Red}}(R, Z, \tau = 0) = 0 \tag{8b}$$

and the boundary conditions at the disk and the ring, respectively (see Fig. 5 for symbols)

$$C_{\mathrm{Ox}}(R, Z, \tau) = 0; \qquad R < 1 \tag{9a}$$

$$\left.\frac{\partial C_{\mathrm{Ox}}(R, Z, \tau)}{\partial Z}\right|_{Z=0} = \xi \left.\frac{\partial C_{\mathrm{Red}}(R, Z, \tau)}{\partial Z}\right|_{Z=0}; \qquad R < 1 \tag{9b}$$

$$C_{\mathrm{Red}}(R, Z, \tau) = 0; \qquad A < R < B \tag{10a}$$

$$\left.\frac{\partial C_{\mathrm{Ox}}(R, Z, \tau)}{\partial Z}\right|_{Z=0} = \xi \left.\frac{\partial C_{\mathrm{Red}}(R, Z, \tau)}{\partial Z}\right|_{Z=0}; \qquad A < R < B \tag{10b}$$

where $A = a/r_{\mathrm{e}}$, $B = b/r_{\mathrm{e}}$, $c^{\mathrm{b}} \equiv c_{\mathrm{Ox}}^{\mathrm{b}}$, $D \equiv D_{\mathrm{Ox}}$, and $\xi \equiv \xi_{\mathrm{Red}} = D_{\mathrm{Red}}/D$. The bulk boundary condition is taken to be reached at $R = R_{\mathrm{G}}$

$$C_{\mathrm{Ox}}(R = R_{\mathrm{G}}, Z, \tau) = 1 \tag{11a}$$

$$C_{\mathrm{Red}}(R = R_{\mathrm{G}}, Z, \tau) = 0 \tag{11b}$$

where $R_{\mathrm{G}} = r_{\mathrm{g}}/r_{\mathrm{e}}$. The symmetry of the problem dictates the following condition

$$\left.\frac{\partial C_{\mathrm{Ox}}(R, Z, \tau)}{\partial R}\right|_{R=0} = \left.\frac{\partial C_{\mathrm{Red}}(R, Z, \tau)}{\partial R}\right|_{R=0} = 0 \tag{12}$$

The boundary conditions at the substrate are

$$\left.\frac{\partial C_{\mathrm{Ox}}(R, Z, \tau)}{\partial Z}\right|_{Z=L} = 0 \tag{13a}$$

$$-\xi \left.\frac{\partial C_{\mathrm{Red}}(R, Z, \tau)}{\partial Z}\right|_{Z=L} = K C_{\mathrm{Red}}(R, Z = L, \tau) \tag{13b}$$

where $L = d/r_{\mathrm{e}}$, and $K = k_{\mathrm{f}} r_{\mathrm{e}}/D$. These boundary conditions imply that Ox does not interact with the substrate under study, but Red transfers irreversibly with rate constant k_{f}, as illustrated in Fig. 3 (c) (which shows the case of iodine transfer, *i.e.* iodide is oxidised at the tip and this oxidised form transfers)

$$\mathrm{Red(w)} \xrightarrow{k_{\mathrm{f}}} \mathrm{Red(o)} \tag{14}$$

The dimensionless currents at the disk, I_D, and ring, I_R, electrodes can be calculated from, respectively

$$I_\mathrm{D} = \frac{I_\mathrm{disk}}{4nFDc^\mathrm{b}r_\mathrm{e}} = \frac{\pi}{2} \int_0^1 R \frac{\partial C_\mathrm{Ox}(R, Z, \tau)}{\partial Z}\bigg|_{Z=0} \mathrm{d}R \qquad (15\mathrm{a})$$

$$I_\mathrm{R} = \frac{I_\mathrm{ring}}{4nFDc^\mathrm{b}r_\mathrm{e}} = \frac{\pi}{2}\xi \int_A^B R \frac{\partial C_\mathrm{Red}(R, Z, \tau)}{\partial Z}\bigg|_{Z=0} \mathrm{d}R \qquad (15\mathrm{b})$$

where I_disk and I_ring are the dimensional currents at the disk and the ring electrodes, respectively.

5.2.2 The numerical solution

The numerical solution used here is based on the finite difference method wherein the simulation domain is discretised to a finite-difference grid. Efficient simulation of a micro-electrode geometry necessitates the use of unequally spaced discretisation points. The discretisation scheme used here is an exponentially expanding mesh as derived by Gavaghan.[168,170,171] Generalised finite difference for arbitrary differencing gives[168]

$$\frac{\partial^2 C_\alpha(R_i, Z_j, \tau)}{\partial R^2} \approx \frac{2\left(h_i C^\tau_{\alpha,i-1,j} - (h_{i-1} + h_i)C^\tau_{\alpha,i,j} + h_{i-1}C^\tau_{\alpha,i+1,j}\right)}{h_{i-1}h_i(h_{i-1} + h_i)} \qquad (16\mathrm{a})$$

$$\frac{\partial C_\alpha(R_i, Z_j, \tau)}{\partial R} \approx \frac{-h_i^2 C^\tau_{\alpha,i-1,j} + (h_i^2 - h_{i-1}^2)C^\tau_{\alpha,i,j} + h_{i-1}^2 C^\tau_{\alpha,i+1,j}}{h_{i-1}h_i(h_{i-1} + h_i)} \qquad (16\mathrm{b})$$

$$\frac{\partial^2 C_\alpha(R_i, Z_j, \tau)}{\partial Z^2} \approx \frac{2\left(k_j C^\tau_{\alpha,i,j-1} - (k_{j-1} + k_j)C^\tau_{\alpha,i,j} + k_{j-1}C^\tau_{\alpha,i,j+1}\right)}{k_{j-1}k_j(k_{j-1} + k_j)} \qquad (16\mathrm{c})$$

The time derivative is obtained as follows

$$\frac{\partial C_\alpha(R_i, Z_j, \tau)}{\partial \tau} \approx \frac{C^{\tau+\Delta\tau/2}_{\alpha,i,j} - C^\tau_{\alpha,i,j}}{\Delta\tau/2} \qquad (17)$$

The solution of the time-dependent problem is obtained with the alternating direction implicit (ADI) method.[172–174] In every half-time step, the ADI algorithm is implicit along one coordinate, with the values for the other coordinate being supplied explicitly from the previous half-time step. The implicit direction is al-

ternated between successive half-time steps. The resulting system of equations has a three-diagonal coefficient matrix and the solution can be obtained with the Thomas algorithm. The current is calculated from[168]

$$I_{\mathrm{D}}(\tau) \approx \frac{\pi}{2} \sum_{\mathrm{disk}} \left(\frac{h_{i-1}}{2} (R_{i-1} \phi_{\mathrm{Ox},i-1}^{\tau} + R_i \phi_{\mathrm{Ox},i}^{\tau}) \right) \tag{18a}$$

$$I_{\mathrm{R}}(\tau) \approx \frac{\xi\pi}{2} \sum_{\mathrm{ring}} \left(\frac{h_{i-1}}{2} (R_{i-1} \phi_{\mathrm{Red},i-1} + R_i \phi_{\mathrm{Red},i}) \right) \tag{18b}$$

where the summation extends over the nodes on the electrode (disk or ring) and

$$\phi_{\alpha,i}^{\tau} = \frac{-k_0^2 C_{\alpha,i,2}^{\tau} + (k_0 + k_1)^2 C_{\alpha,i,1}^{\tau} - (k_1^2 + 2k_0 k_1) C_{\alpha,i,0}^{\tau}}{k_0 k_1 (k_0 + k_1)} \tag{19}$$

The ADI method is known to give initial oscillations in the current that can be removed if sufficiently small time steps are used.[170] These oscillations are due to the singularity in the boundary condition at the electrode (a potential step). However, it not efficient to use such a short time-step throughout the simulation and, therefore, an expanding time-step was used. In practice, this was achieved by multiplying the time-step by a constant, γ, after a suitable number of time-steps, M. The initial time step was chosen to be $dT_0 = \min\{h_{\min}, k_{\min}\}^2$ which effectively removed oscillations from the current transient.

The spatial grid is expanded in an exponential fashion; following Amphlett and Denuault,[154] the grid in Z-direction is expanded both from the tip and the substrate

$$
\begin{aligned}
k_0 &= k_{\min} \\
k_j &= f k_{j-1} \quad ; \qquad j = 1, \ldots, K_{\max}/2 - 1 \\
k_{K_{\max}-1} &= k_{\min} \\
k_j &= f k_{j+1} \quad ; \qquad j = K_{\max}/2, \ldots, K_{\max} - 2
\end{aligned} \tag{20}
$$

where $k_{\min}$ is the minimum element size, f is the expansion factor and $K_{\max}$ is the number of node points in Z-direction. Similarly, in R-direction, for a microdisk

electrode

$$h_{H-1} = h_{\min}$$
$$h_i = fh_{i+1} \quad ; \qquad i = 1, \ldots, H-2$$
$$h_H = h_{\min}$$
$$h_i = fh_{i-1} \quad ; \qquad i = H+1, \ldots, H_{\max} - 1 \qquad (21)$$

where $h_{\min}$ is the minimum element size, H is the number of nodes over the electrode, and $H_{\max}$ is the total number of nodes along the R-coordinate. For a micro ring-disk electrode, the grid was generated as follows

$$h_{H-1} = h_{\min}$$
$$h_i = fh_{i+1} \quad ; \qquad i = 1, \ldots, H-2$$
$$h_H = h_{\min}$$
$$h_i = fh_{i-1} \quad ; \qquad i = H+1, \ldots, (H+HA)/2 - 1$$
$$h_{HA-1} = h_{\min}$$
$$h_i = fh_{i+1} \quad ; \qquad i = (H+HA)/2, \ldots, HA-2$$
$$h_{HA} = h_{\min}$$
$$h_i = fh_{i-1} \quad ; \qquad i = HA+1, \ldots, (HA+HB)/2 - 1$$
$$h_{HB-1} = h_{\min}$$
$$h_i = fh_{i+1} \quad ; \qquad i = (HA+HB)/2, \ldots, HB-2$$
$$h_{HB} = h_{\min}$$
$$h_i = fh_{i-1} \quad ; \qquad i = HB+1, \ldots, H_{\max} - 1 \qquad (22)$$

The finite difference grids produced by Eqs. (21) and (22) are shown in Fig. 6.

5.3   Results and Discussion

In order to quantify the accuracy of the presented numerical solution, the solution is compared to known limiting cases and approximations, transients at both micro disk and ring electrodes and conventional SECM approach curves.
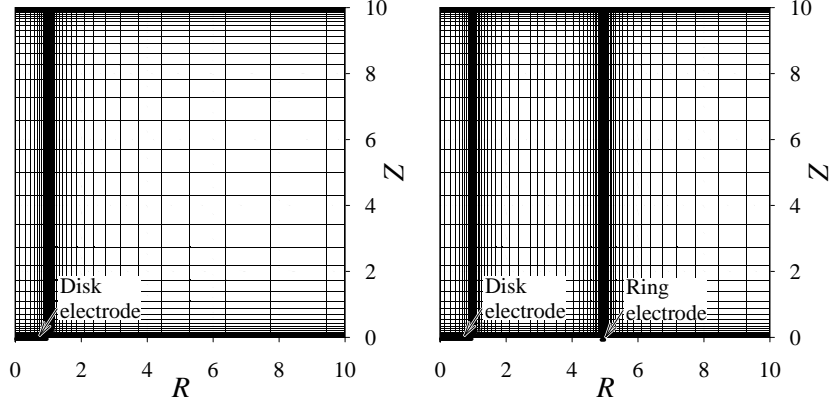
Figure 6: The grids used in SECM simulations (left) and RD-SECM (right). Both with following parameters: $R_\mathrm{G} = 10$, $L = 10$, $h_\mathrm{min} = k_\mathrm{min} = 10^{-2}$, $f = 1.25$, and the RD-SECM, $A = 4.9$, and $B = 5.0$.

5.3.1 Potential step at a disk microelectrode

The dimensionless diffusion limited current at a microdisk electrode for short and long times, respectively, can be calculated from[175]

$$I_\mathrm{D} = \frac{\pi^{1/2}}{2T^{1/2}} + \frac{\pi}{4} + 0.094T^{1/2} \tag{23a}$$

$$I_\mathrm{D} = 1 + 0.71835T^{-1/2} + 0.05626T^{-3/2} - 0.00646T^{-5/2} \tag{23b}$$

where $T = 4\tau = 4Dt/r_\mathrm{e}^2$. Shoup and Szabo proposed an approximation for the current response of the Cottrell experiment that is accurate to 0.6% for all times[176]

$$I_\mathrm{D} = 0.7854 + 0.8862T^{-1/2} + 0.2146\exp(-0.7823T^{-1/2}) \tag{24}$$

A computed transient is compared to the values given by the Shoup-Szabo equation in Fig. 7 (a). The percentage difference between the numerical solution and Eqs. (23a), (23b), and (24) is shown Fig. 7 (b). Comparing the limiting cases and the Shoup-Szabo equation, it is likely that the S-shape difference between the present solution and Shoup-Szabo equation reflects the error in that approximation rather than the error in the present simulation. Indeed, it is likely that the calculated transient is accurate to within 0.2% based on a comparison with the limiting cases Eq. (23a) and Eq. (23b). It is of interest to note in Fig. 7 (a) that two different

32

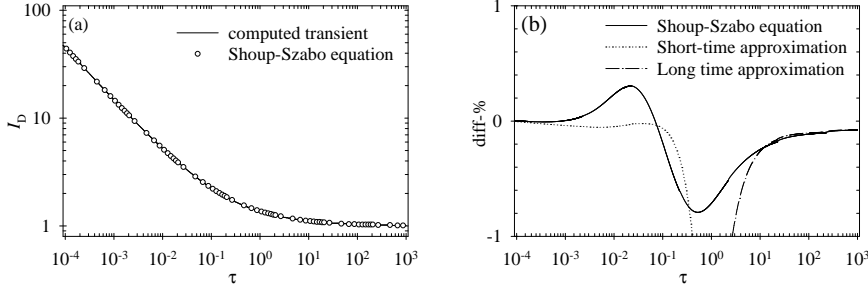*Figure 7*: (a) Comparison between the calculated transient with $h_{\min} = k_{\min} = 10^{-4}$, $f = 1.1$, $R_{\mathrm{G}} = L = 100$ and the Shoup-Szabo equation, Eq. (24) ($\circ$). (b) the difference between the calculated transient and the Shoup-Szabo equation (—), Eq. (24), the short time limit ($\cdots$), Eq. (23a), and the long time limit (–·–), Eq. (23b).

Figure 8: The difference (in percent) between the computed transient and the short time Eq. (23a) and long time Eq. (23b) limiting cases: the effect of changing the expansion coefficient, with $f = 1.25$ (—), 1.175 ($\cdots$), 1.15 (–·–) and 1.1 (–··–), $h_{\min} = k_{\min} = h_0 = 10^{-4}$ (a) and $h_{\min} = k_{\min} = h_0 = 10^{-5}$ (b). All with $M = 4000$ and $\gamma = 10$.

time domains can be distinguished: at short times ($\tau < 10^{-2}$), the slope of the current transient in this logarithmic plot is $1/2$, which reflects the fact that the diffusion field can be approximated as linear at such short times. On the other hand, at longer times ($\tau > 10^{2}$), the dimensionless current tends to the limiting value of 1 as the system approaches steady-state.

The effect of the minimum element size and the expansion factor are investigated in Fig. 8 for the case of a diffusion controlled potential step at an UME in the bulk of a solution. Fig. 8 (a) and (b) show the effect of the expansion factor for two different element sizes, $h_{\min} = 10^{-4}$ and $h_{\min} = 10^{-5}$; due to the choice $dT_0 = \min\{h_{\min}, k_{\min}\}^2$, the smaller the chosen $h_{\min}$, the shorter the times that can be examined. As was noted previously,[168] there is a choice of $f \neq 1$ that optimises the error cancelling effect. It can be seen that for $h_{\min} = 10^{-4}$, this op-
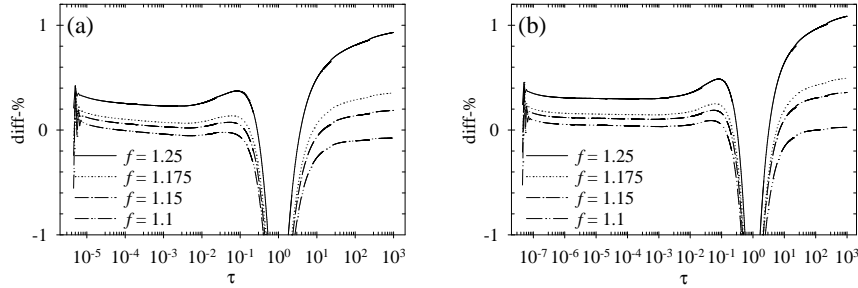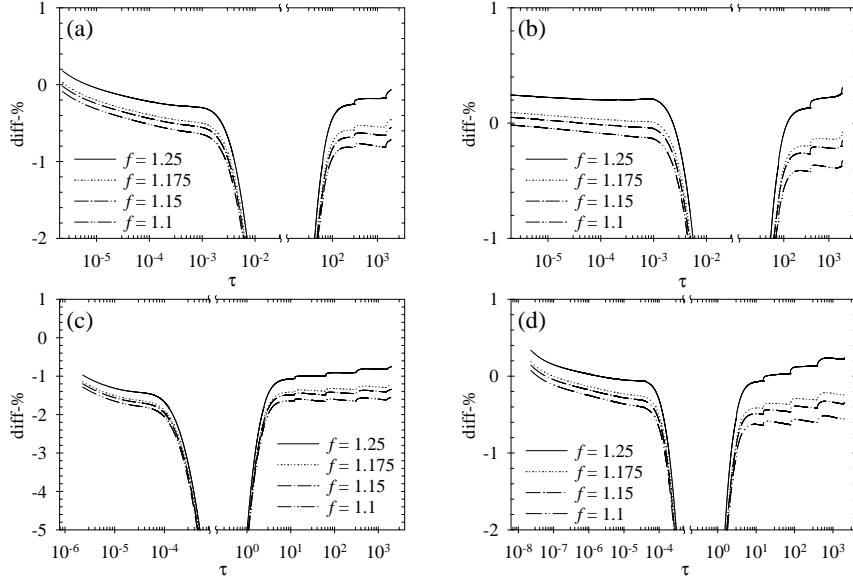
Figure 9: The difference (in percent) between the computed transient at a ring electrode and the short time Eq. (27) and long time Eq. (25) limiting cases: The effect of changing the expansion coefficient, with $h_{\min} = 10^{-4}$ (a), (c) and $h_{\min} = 10^{-5}$ (b), (d) and $f = 1.25$ (—), 1.175 ($\cdots$), 1.15 (–·–), and 1.1 (–··–). (a) and (b) with $A = 9.9$, $B = 10.0$, (c) and (d) with $A = 1.98$, $B = 2.0$. All with $M = 5000$ and $\gamma = 5$.

timum is for $f = 1.15$ whereas for $h_{\min} = 10^{-5}$, $f = 1.1$ yields even better results. In general, it can be concluded that appropriate choice of mesh parameters yield errors smaller than 0.2% throughout the computed transient.

5.3.2 Potential step at a ring microelectrode

The diffusion limited current to a microring electrode at long times is given by the following equation[177]

$$I_{\mathrm{R}} = l_0 \left(1 + 2l_0 (\pi^3 T)^{-1/2} \right) \tag{25}$$

where

$$l_0 = \frac{\pi^2}{4} \frac{A + B}{\ln\left(32A/(B - A) + \exp(\pi^2/4) \right)} \tag{26}$$

The short time behaviour can be deduced from a general treatment by Oldham[178–180]

$$I_{\mathrm{R}} = \frac{\pi(A + B)(B - A)}{4} \left((\pi T)^{-1/2} + (B - A)^{-1} \right) \tag{27}$$

34

Fig. 9 shows the effect of the expansion factor and minimum element size on the ring electrode transient as compared to the limiting cases given by Eq. (25) and Eq. (27). Fig. 9 shows simulations for two different sized ring electrodes, one with $A = 9.9$ and $B = 10.0$, (a) and (b), and the other with $A = 1.98$ and $B = 2.0$, (c) and (d). The latter of the rings is rather small and thin, and it is therefore anticipated that it has more stringent requirements for the simulation than the larger electrode. The choice of normalisation was dictated by the fact that these simulations will ultimately be used for RD-SECM calculations. It can be clearly seen that, due to the thinness of the rings considered, the minimum element size has to be rather small for accurate results. From Fig. 9, it can be concluded that $h_{\min} = k_{\min} = 10^{-5}$ and $f = 1.175$ or $f = 1.15$ constitute appropriate parameter values for these ring simulations. A similar conclusion was reached very recently by Compton *et al.*, who used the same differentiation scheme to simulate the steady-state, chronoamperometry and cyclic voltammetry at ring electrodes.[181] It should be borne in mind, however, that all the values of the expansion coefficient considered yield errors smaller than 1% (for $h_{\min} = k_{\min} = 10^{-5}$) which can be considered to be the experimentally attainable level of accuracy.

5.3.3   SECM approach curves

The present numerical solutions will be compared to the analytical solutions provided by Galceran *et al.*[169] who were able to retain the effect of the overall tip radius in their results. They obtained the approach curve as a solution to a linear system. A *Mathematica* notebook providing the solution can be obtained from the web page *www.udl.es/usuaris/q4088428/*.

Fig. 10 shows a comparison between the present simulations and the exact results provided by the treatment of Galceran *et al.*. It can be seen that with both minimum element sizes considered, there exists an optimum choice of the expansion factor: $f = 1.15$ for $h_{\min} = 10^{-4}$ and $f = 1.1$ for $h_{\min} = 10^{-5}$. Furthermore, the results for an approach to an insulator show that the error increases at short separations. However, as the current tends to zero, the absolute error remains small, but the relative error increases. For the same reason, the relative error on approach curves to a conductor decreases at short tip-substrate separations. This is further elaborated in Fig. 11 where the absolute errors are shown.

35
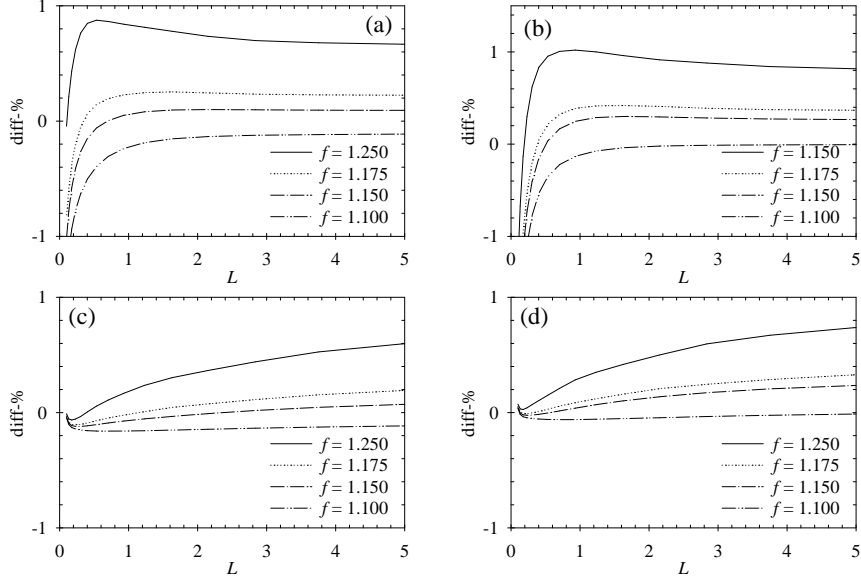
Figure 10: The difference (in percent) between the computed approach curve and the theory by Galceran *et al.*[169] Approach to an insulating substrate, (a) and (b), and to a conducting substrate, (c) and (d). The element size $h_{\min} = k_{\min} = 10^{-4}$, (a) and (c), and $h_{\min} = k_{\min} = 10^{-5}$, (b) and (d). The effect of different expansion factors, $f = 1.250$ (—), 1.175 ($\cdots$), 1.150 (-·-), and 1.100 (− · ·−). All with $\gamma = 5$, $M = 4000$, and $R_{\mathrm{G}} = 10$.

Galceran *et al.* also provide approximate "zeroth order" expressions and point out that they are more accurate than the equations given by Mirkin *et al.*[182] The approximations provided by Mirkin *et al.* are, for an insulating substrate

$$I_{\mathrm{D}}^{\mathrm{insl}} = \frac{1}{0.15 + 1.5385/L + 0.58\exp(-1.14/L) + 0.0908\exp((L-6.3)/1.017L)} \tag{28}$$

and a conducting substrate

$$I_{\mathrm{D}}^{\mathrm{cond}} = 0.78377/L + 0.3315\exp(-1.0672/L) + 0.68 \tag{29}$$

Fig. 11 shows a comparison between the these simulations and the results of Galceran *et al.* for the actual approach curves, and the correspondence is seen to be excellent. Also shown are the approach curves based on the approximation by Mirkin *et al.* and, as noted by Galceran *et al.*, they are slightly inaccurate. However, it would be difficult to detect this experimentally. The present results have not been compared with the simulation by Amphlett and Denuault,[154] as
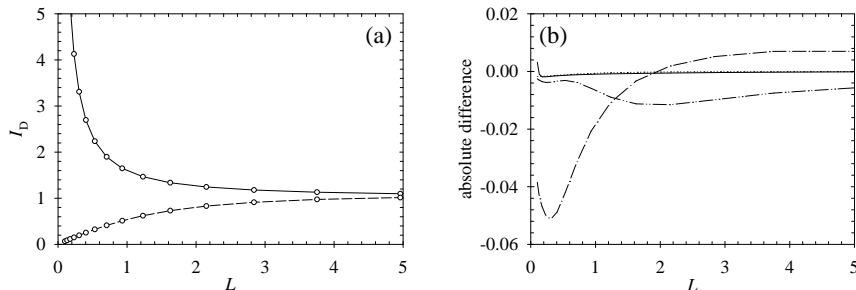
Figure 11: (a) The computed approach curves for both insulating and conducting substrates (full lines) and the values obtained from the theory by Galceran *et al.* (○). (b) the absolute difference between the solution due to Galceran *et al.* and the computed approach curve (insulating (—) and conducting (···) substrates) and the Mirkin approximation, Eqs. (28) and (29), (insulating (–·–) and conducting (–··–) substrates).

the simulation domain used was different, *i.e.* the effect of finite R_G was taken into account by extending the simulation domain to allow for diffusion behind the plane of the electrode, that is, so-called back diffusion.

5.3.4 RD-SECM: Comparison between ADI and FEM calculations

Finally, to check the accuracy of the RD-simulations, some results were compared with finite element simulations. These simulations were done with Matlab's FEM-LAB finite element package with a adaptively refined grid algorithm. The results are shown in Fig. 12 and it can be seen that there is perfect correspondence between the two different numerical methods. The simulation compared were for a thin ring electrode as it is anticipated that this is numerically more demanding than a thicker ring. In addition, the experimental system presented in Publs. III and IV is a thin-ring configuration.

5.3.5 Probing partitioning with RD-SECM

The simulations presented in the previous sections establish the merits of using arbitrary differentiation: high accuracy can be obtained with a small number of elements on different geometries. The expansion coefficient has an optimum choice that depends on the minimum element size and the type of experiment that is simulated. In light of the present calculations, for RD-SECM simulations,
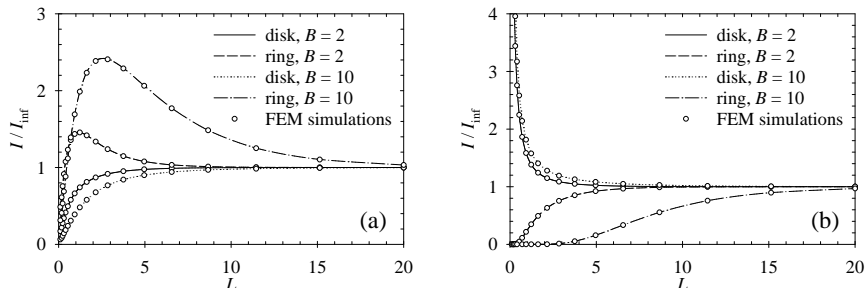
Figure 12: Approach curves for DG/RC RD-SECM, comparison between the present ADI simulations (lines) and FEM calculations (○). The values of parameters used: $B = 2$ (disk (—) and ring (- -)) or $B = 10$ (disk (⋯) and ring ($- \cdot -$)). All curves with $A/B = 0.990$, $R_G = B + 5$, $h_{\min} = k_{\min} = 10^{-5}$, $f = 1.1$, $\gamma = 5$, and $M = 5000$.

such pairs of values are $f = 1.15$, $h_{\min} = 10^{-4}$ and $f = 1.10$, $h_{\min} = 10^{-5}$. The presented algorithm will now be used to consider a partitioning process at a liquid | liquid interface using RD-SECM.

In a disk-generation/ring-collection experiment at RD-SECM, the current response at the disk is as expected for a conventional disk SECM tip: negative feedback for an approach to an insulator due to hindered reactant diffusion at the tip and positive feedback for an approach to a conductor due to reactant regeneration.[136] For the collector ring electrode, as the tip approaches an insulator (Fig. 3 (a)), diffusion of Red away from the disk is blocked by the substrate and initially, the ring current increases. However, at closer distances, the ring current decreases as the amount of disk-generated Ox is reduced. In contrast, for an approach to a conducting substrate (Fig. 3 (b)), the concentration changes due to the reaction at the disk are localised in the disk-substrate gap and, thus the collection current at the ring decreases to zero, as positive feedback at the disk increases. The partitioning process under investigation is depicted in Fig. 3 (c). Iodide reacts at the disk electrode to yield iodine (in contrast to Fig. 3 (a) and (b), iodide is oxidised), which is reduced back to iodide at the ring electrode. Due to its very hydrophilic nature, iodide will not cross the liquid | liquid interface. However, iodine is much more soluble in organic solvents than in water and can therefore be thought to transfer irreversibly, in a thermodynamic sense. Nevertheless, it is possible to envision an existence of a kinetic barrier and this was included in the model.

Typical simulated responses for DG/RC RD-SECM as a function of the par-

38
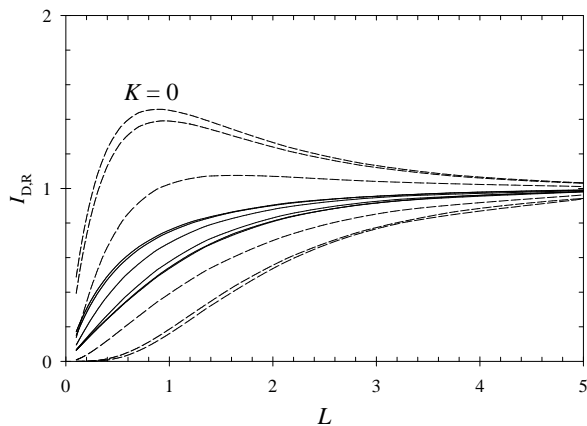
Figure 13: Approach curves for DG/RC RD-SECM with an irreversible transfer occurring at the substrate, from top to bottom, for $K = 0$, 0.01, 0.1, 1.0, 10.0, and 100.0. The disk response is given by the solid line and the ring by the dashed line. The values of parameters used: $B = 2$, $A/B = 0.990$, $R_{\mathrm{G}} = 7$, $h_{\min} = k_{\min} = 10^{-5}$, $f = 1.1$, $\gamma = 5$, and $M = 5000$.

titioning rate constant are shown in Fig. 13. If the rate constant for partition reaction is 0, the response of an insulating substrate is regained. On the other hand, with finite rate constants, the disk generated iodine transfers into the organic phase and consequently, the ring response tends to the response at a conducting substrate. The disk response is also sensitive to the partitioning, changing from the RD-SECM insulator response to one that is equal to the response from an SECM tip with a certain R_{G} without a ring electrode; if the partitioning is fast, the disk generated species escapes into the other phase and ring electrode has no effect on the disk response. The sensitivity of RD-SECM with respect to partitioning kinetics was investigated by considering different limiting cases: thin or thick ring, small or large ring radius. The results are shown in Table 1. Tentatively, the results can be summarised as follows: the maximum discernible value of the dimensionless rate constant is ~ 10 irrespective of the electrode geometry. The minimum detectable rate constant depends on the electrode geometry and it would seem that the thinner and the larger the ring is, the better the sensitivity. The experimental ring size is limited by, for example, the ability to approach the interface under study and time to reach a steady-state, and cannot be increased much above 10. The maximum sensitivity of the method would therefore appear to be of the order of 10^{-3}. The dimensionless rate constant is related to the real

Table 1: The sensitivity (minimum and maximum discernible rate constants) of RD-SECM in probing a partition reaction.

B	A/B	$K(\text{min})$	$K(\text{max})$
2	0.99	5.00×10^{-3}	10
10	0.99	1.00×10^{-3}	10
2	0.75	1.00×10^{-2}	10
10	0.75	5.00×10^{-3}	10

rate constant through $K = k_{\text{f}}r_{\text{e}}/D$. For a 25μm diameter disk electrode and for a typical value of $D = 10^{-5}\text{cm}^2/\text{s}$, the upper and lower limits of rate constant are 0.08cm/s and $8.0 \times 10^{-6}\text{cm/s}$. For a much smaller electrode, $r_{\text{e}} = 0.5\mu$m, the upper and lower limits are 2.0cm/s and $2.0 \times 10^{-4}\text{cm/s}$. These are similar or higher compared to the sensitivity reported for DPSC-SECM[70, 71] and, remarkably, obtainable with a steady-state measurement.

Experimental results DG/RC RD-SECM at water | DCHx interface were measured in a manner described in Publ. IV and the results are shown in Fig. 14. The solution contained simultaneously iodide and $\text{Ru(NH}_3)_6^{3+}$ and the tip employed consisted of 12.5μm radius Pt disk with a Au ring electrode prepared by sputtering. Fig. 14 shows the response when $\text{Ru(NH}_3)_6^{3+}$ is reduced at the disk and the generated $\text{Ru(NH}_3)_6^{2+}$ is re-oxidised at the ring electrode: neither species can transfer across the liquid | liquid interface and the typical insulator response is obtained. The full line is a simulated response with the parameter values of $B = 7$, $A/B = 0.990$, and $R_{\text{G}} = 13$. The diameter and the thickness of the ring electrode are consistent with limiting currents obtained from cyclic voltammetry (data not shown). The slight deviation between the experimental and theoretical ring response is probably due to the approach speed; as elaborated in Publ. IV, large ring electrodes require rather low approach speeds to yield a true steady-state response.

Fig. 14 (b) shows the results of a similar experiment wherein iodide is oxidised at the disk and the generated iodine is reduced back to iodide at the ring. The disk response shows similar negative feedback behaviour to the previous measurement while the ring response is characteristic of strong partitioning of the disk-generated species. The ring response can be modelled by diffusion controlled transfer of iodine across the liquid | liquid interface apart from fairly close tip-interface separations.
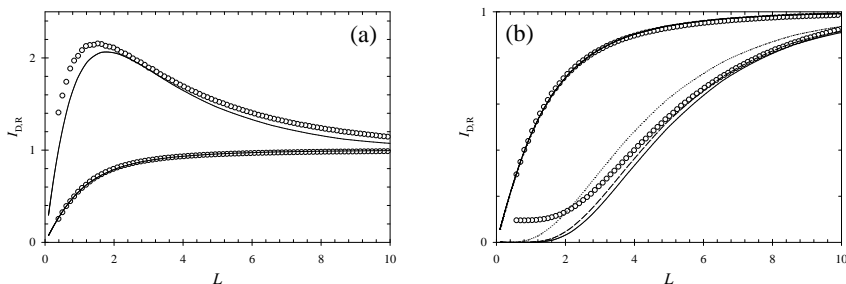
Figure 14: Experimental approach curves to a membrane supported 1,6-DCHx-water interface. The circles show experimental results for (a) 3.1 mM $Ru(NH_3)_6^{3+}$ in 200 mM LiCl that does not partition into the organic phase, with the disk biased at -0.35 V vs Ag/AgCl and the ring at 0.0 V vs Ag/AgCl and (b) 3.2 mM iodide solution (200 mM LiCl) with the disk held at 0.6 V vs Ag/AgCl and the ring at 0.0 V vs Ag/AgCl. Disk radius was 12.5μm and the approach speed 0.7 μm/s. The solid lines show insulator response (a) and diffusion controlled partitioning behaviour (b) with the parameter values $B = 7$, $A/B = 0.990$, $R_G = 13$, $f = 1.15$, $h_{min} = 10^{-4}$, $\gamma = 5$, and $M = 5000$. The dashed line shows the theoretical response with a partition rate constant of $K = 5$ and the dotted line with $K = 1$.

It is likely that the observed discrepancy is due to establishment of a partition equilibrium between the iodine in the aqueous and in the organic phases, respectively. The dashed and dotted lines show the ring response with a finite partitioning rate constants but this does not significantly improve the correspondence between the theoretical and experimental results compared to the diffusion limited response.

In conclusion, SECM experiments have been modelled with the arbitrary finite difference scheme as described by Gavaghan.[168] It was noted to be well-suited to different experimental geometries (disk and ring electrodes) and was computationally efficient. A model was developed for DG/RC RD-SECM experiment wherein the disk generated species can irreversibly transfer across a liquid | liquid interface. Based on fitting the theory to experimental results it can be concluded that iodine partitioning across a water | DCHx interface is fast and RD-SECM response was close to diffusion limited ($k_f > 0.05$cm/s). Further refining the model to include attainment of a partitioning equilibrium will be considered in the future.

6 Conclusions

This thesis presents novel approaches to old, existing problems in liquid | liquid electrochemistry, introducing means to control the mass transfer at these interfaces, to control the state of adsorbed monolayers, and to probe reactivity of non-charged or possibly short-lived species.

The first paper of this thesis demonstrated the application of a well-defined channel flow geometry to the study of charge transfer at an immobilised liquid | liquid interface. The linear diffusion in the gelled organic phase and the convective diffusion in the aqueous phase yielded an asymmetric voltammetric response that provided clear diagnostic criteria concerning the direction of ion transfer. The experimental results were in good correspondence with theoretical simulations of both a simplified Singh-Dutt approach and a full, two-dimensional model.

In subsequent work, a unique combination of the LB technique with an electrochemical cell as a substrate was proposed. This method was used to deposit phospholipid monolayers at the water | NPOE interface in a controlled and reproducible manner. The resulting monolayer-modified interface was characterised in terms of the interfacial capacitance and ion permeability. While addition of the monolayer significantly altered the capacitive behaviour of the interface, cyclic voltammetric measurements could not detect an effect on the rate of ion transfer. The capacitance data was interpreted with a simple three-layer electrostatic model.

The latter part of this thesis concerns probing reactivity at liquid | liquid interfaces. For the first time, a micro ring-disk electrode was used as an SECM probe. This makes it possible to simultaneously monitor the interactions of two different species with a target interface in a steady-state measurement. A proposed mode of operation, disk-generation/ring-collection SECM, was characterised both experimentally and theoretically in the limiting cases of perfectly insulating or conducting substrates. DG/RC SECM was consequently applied to study a partitioning process at a liquid | liquid interface that involves no net charge transfer. Based on a refined theoretical model where the disk-generated species is allowed to irreversibly transfer across the interface, it was concluded that the minimum rate constant for iodine partitioning across a water | DCHx interface is 0.05cm/s. The results also showed that a model allowing for a partitioning equilibrium may

provide a more accurate description of the transport problem.

Another report proposed the use of a Pt coated micropipette supported liquid | liquid interface to study the lipophilicity of electrogenerated species. This method was applied to investigate ions that would be difficult to obtain commercially or to synthesise chemically due to lability. This was achieved by *in situ* localised electrolysis of the neutral reactant at the Pt coat electrode in the vicinity of a polarised liquid | liquid interface. The lipophilicity of the generated charged species was then probed by measuring the transfer potential across the liquid | liquid interface. The proposed method was noted to be facile, to require only very small volumes of both phases, and to enable the study of potentially unstable charged products of electron transfer reactions.

List of Abbreviations

ADI	alternating direction implicit
AFM	atomic force microscopy
BEM	boundary element method
CFC	channel-flow cell
CVD	chemical vapour deposition
DCE	1,2-dichloroethane
DCHx	1,6-dichlorohexane
DG/RC	disk-generation/ring-collection
DPPC	dipalmitoyl phosphatidylcholine
DPSC	double potential step chronoamperometry
DSPC	distearoyl phosphatidylcholine
DPV	differential pulse voltammetry
EDE	electrolyte dropping electrode
ET	electron transfer
FEM	finite element method
FIT	facilitated ion transfer
ISE	ion-selective electrode
IT	ion transfer
ITIES	interface between two immiscible electrolyte solutions
LB	Langmuir-Blodgett
$Lu(PC)_2$	lutetium bisphthalocyanine
MD	molecular dynamics
MEMED	microelectrochemical measurements at expanding droplets
NPOE	nitrophenyl octyl ether
PTFE	poly(tetrafluoroethene)
PVC	poly(vinylchloride)
QELS	quasi-elastic light scattering
RD	ring-disk
RDC	rotating diffusion cell
$Ru(TPP)(py)_2$	bis(pyridine)-tetraphenylporphyrinatoruthenium
SECM	scanning electrochemical microscopy/microscope
SFG	sum-frequency generation
SHG	second-harmonic generation
SPM	scanning probe microscopy
STM	scanning tunneling microscope
TCNQ	tetracyanoquinodimethane
TEA^+	tetraethyl ammonium cation
UME	ultramicroelectrode

List of Symbols

$\Delta_\mathrm{o}^\mathrm{w}\phi$	Galvani potential difference between the phases
$\Delta_\mathrm{o}^\mathrm{w}\phi_i^0$	standard transfer potential of ion i
$\Delta\tau$	dimensionless time-step
$\Delta G_{i,\mathrm{tr.}}^{\mathrm{w}\rightarrow\mathrm{o}}$	standard Gibbs free energy of transfer of ion i
γ	multiplication factor of the time-step
$\mu_i^{0,\mathrm{o}}$	standard chemical potential of ion i the organic phase
$\mu_i^{0,\mathrm{w}}$	standard chemical potential of ion i the aqueous phase
τ	dimensionless time
ξ_i	scaled diffusion coefficient of ion i, $\xi_i = D_i/D$
c_i	concentration of species i
c^b	bulk concentration of the initially present species
C_i	dimensionless concentration of species i
d	distance from the substrate
dT_0	initial dimensionless time-step
D_i	diffusion coefficient of species i
f	grid expansion factor
F	Faraday constant
h_i	ith element in the radial direction
I_disk	disk current
I_D	dimensionless disk current
I_ring	ring current
I_R	dimensionless ring current
H	number of elements over the disk electrode
H_max	number of elements in radial direction
k_f	rate constant of the partitioning reaction
k_j	jth element in the z-direction
K	dimensionless rate constant of the partitioning reaction
$K(\mathrm{min})$	minimum discernible dimensionless partitioning rate constant
$K(\mathrm{max})$	maximum discernible dimensionless partitioning rate constant
K_max	number of elements in z-direction
L	dimensionless distance from the substrate
M	number of time-steps before multiplication by a factor of γ
r_e	radius of the disk electrode
r_g	overall tip radius
R	dimensionless radial coordinate
R_G	dimensionless overall tip radius
t	time
T	dimensionless time, $T = 4\tau$
z_i	charge of ion i
Z	dimensionless z-coordinate

References

[1] C. Gavach, *C. R. Acad. Sci., Ser. C* **269** (1969) 1356–1359.

[2] C. Gavach, P. Seta, F. Henry, *Bioelectrochem. Bioenerg.* **1** (1974) 329–342.

[3] J. Koryta, P. Van'ysek, M. Brezina, *J. Electroanal. Chem. Interfacial Electrochem.* **67** (1976) 263–266.

[4] Z. Samec, V. Mareček, J. Koryta, M. W. Khalil, *J. Electroanal. Chem. Interfacial Electrochem.* **83** (1977) 393–397.

[5] C. Gavach, P. Seta, B. D'Epenoux, *J. Electroanal. Chem. Interfacial Electrochem.* **83** (1977) 225–235.

[6] J. Koryta, *Electrochim. Acta* **24** (1979) 293–300.

[7] B. D'Epenoux, P. Seta, G. Amblard, C. Gavach, *J. Electroanal. Chem. Interfacial Electrochem.* **99** (1979) 77–84.

[8] J. Koryta, M. Brezina, A. Hofmanová, D. Homolka, L. Q. Hung, W. Khalil, V. Mareček, Z. Samec, S. K. Sen, P. Vanýsek, J. Weber, *Bioelectrochem. Bioenerg.* **7** (1980) 61–68.

[9] D. Homolka, L. Q. Hung, A. Hofmanová, M. W. Khalil, J. Koryta, V. Mareček, Z. Samec, S. K. Sen, P. Vanýsek, J. Weber, M. Březina, M. Janda, I. Stibor, *Anal. Chem.* **52** (1980) 1606–1610.

[10] A. Mälkiä, P. Liljeroth, A.-K. Kontturi, K. Kontturi, *J. Phys. Chem. B* **105** (2001) 10884–10892.

[11] C. Johans, R. Lahtinen, K. Kontturi, D. J. Schiffrin, *J. Electroanal. Chem.* **488** (2000) 99–109.

[12] C. Johans, K. Kontturi, D. J. Schiffrin, *J. Electroanal. Chem.* **526** (2002) 29–35.

[13] G. Taylor, H. H. Girault, *J. Electroanal. Chem.* **208** (1986) 179–183.

[14] J. A. Campbell, H. H. Girault, *J. Electroanal. Chem. Interfacial Electrochem.* **266** (1989) 465–469.

[15] M. C. Osborne, Y. Shao, C. M. Pereira, H. H. Girault, *J. Electroanal. Chem.* **364** (1994) 155–161.

[16] M. Senda, T. Kakiuchi, T. Osakai, *Electrochim. Acta* **36** (1991) 253–262.

[17] H. J. Lee, C. Beriet, H. H. Girault, *J. Electroanal. Chem.* **453** (1998) 211–219.

[18] H. J. Lee, H. H. Girault, *Anal. Chem.* **70** (1998) 4280–4285.

[19] S. Sawada, H. Torii, T. Osakai, T. Kimoto, *Anal. Chem.* **70** (1998) 4286–4290.

[20] B. Liu, M. V. Mirkin, *Anal. Chem.* **73** (2001) 670A–677A.

[21] H. H. J. Girault, D. J. Schiffrin, Charge transfer through phospholipid monolayers adsorbed at liquid-liquid interfaces, *in:* Charge and Field Effects Biosystems, M. J. Allen, P. N. R. Usherwood (Eds.), Abacus Press, Tunbridge Wells, 1984, pp. 171–178.

[22] T. Kondo, T. Kakiuchi, M. Senda, *Anal. Sci.* **7** (1991) 1725–1728.

[23] T. Kondo, T. Kakiuchi, M. Senda, *Biochim. Biophys. Acta* **1124** (1992) 1–6.

[24] T. Kondo, T. Kakiuchi, M. Senda, *Bioelectrochem. Bioenerg.* **34** (1994) 93–100.

[25] L. M. Yudi, E. Santos, A. M. Baruzzi, V. M. Solis, *J. Electroanal. Chem.* **379** (1994) 151–158.

[26] Y. Cheng, D. J. Schiffrin, *J. Chem. Soc., Faraday Trans.* **90** (1994) 2517–2523.

[27] Y. Cheng, D. J. Schiffrin, *J. Chem. Soc.-Faraday Trans.* **92** (1996) 3865–3871.

[28] R. M. Lahtinen, D. J. Fermin, H. Jensen, K. Kontturi, H. H. Girault, *Electrochem. Commun.* **2** (2000) 230–234.

[29] J. Zhang, R. M. Lahtinen, K. Kontturi, P. R. Unwin, D. J. Schiffrin, *Chem. Commun.* (2001) 1818–1819.

[30] D. J. Fermin, H. D. Duong, Z. F. Ding, P. F. Brevet, H. H. Girault, *Electrochem. Commun.* **1** (1999) 29–32.

[31] H. Jensen, D. J. Fermin, H. H. Girault, *Phys. Chem. Chem. Phys.* **3** (2001) 2503–2508.

[32] K. Kontturi, L. Murtomäki, *J. Pharm. Sci.* **81** (1992) 970–975.

[33] F. Reymond, G. Steyaert, P. A. Carrupt, B. Testa, H. Girault, *J. Am. Chem. Soc.* **118** (1996) 11951–11957.

[34] F. Reymond, G. Steyaert, P. A. Carrupt, D. Morin, J. P. Tillement, H. H. Girault, B. Testa, *Pharm. Res.* **16** (1999) 616–624.

[35] V. Chopineaux-Courtois, F. Reymond, G. Bouchard, P. A. Carrupt, B. Testa, H. H. Girault, *J. Am. Chem. Soc.* **121** (1999) 1743–1747.

[36] F. Reymond, V. Chopineaux-Courtois, G. Steyaert, G. Bouchard, P. A. Carrupt, B. Testa, H. H. Girault, *J. Electroanal. Chem.* **462** (1999) 235–250.

[37] F. Reymond, P. A. Carrupt, B. Testa, H. H. Girault, *Chem.-Eur. J.* **5** (1999) 39–47.

[38] G. Caron, G. Steyaert, A. Pagliara, F. Reymond, P. Crivori, P. Gaillard, P. A. Carrupt, A. Avdeef, J. Comer, K. J. Box, H. H. Girault, B. Testa, *Helv. Chim. Acta* **82** (1999) 1211–1222.

[39] V. Gobry, S. Ulmeanu, F. Reymond, G. Bouchard, P. A. Carrupt, B. Testa, H. H. Girault, *J. Am. Chem. Soc.* **123** (2001) 10684–10690.

[40] A. G. Volkov, D. W. Deamer (Eds.), Liquid-Liquid Interfaces; Theory and Methods, CRC Press, Boca Raton, 1996.

[41] A. G. Volkov (Ed.), Liquid Intefaces in Chemical, Biological and Pharmaceutical Applications, Marcel Dekker, New York, 2001.

[42] H. H. Girault, Charge Transfer Across Liquid-Liquid Interfaces, *in:* Modern Aspects of Electrochemistry, Vol. 25, J. O. Bockris, B. E. Conway, R. E. White (Eds.), Plenum Press, New York, 1993, pp. 1–62.

[43] H. H. Girault, D. J. Schiffrin, Electrochemistry of Liquid-Liquid Interfaces, *in:* Electroanalytical Chemistry, Vol. 15, A. J. Bard (Ed.), Marcel Dekker, New York, 1989, pp. 1–141.

[44] P. Vanýsek, Liquid-Liquid Electrochemistry, *in:* Modern Electroanalytical Techniques, Vol. 139, P. Vanysek (Ed.), John Wiley & Sons, New York, 1996, pp. 337–364.

[45] A. G. Volkov, D. W. Deamer, D. L. Tanelian, V. S. Markin, Liquid Interfaces in Chemistry and Biology, John Wiley & Sons, New York, 1998.

[46] D. A. Higgins, R. M. Corn, *J. Phys. Chem.* **97** (1993) 489–493.

[47] R. M. Corn, D. A. Higgins, *Chem. Rev.* **94** (1994) 107–125.

[48] J. C. Conboy, J. L. Daschbach, G. L. Richmond, *J. Phys. Chem.* **98** (1994) 9688–9692.

[49] A. A. T. Luca, P. Hebert, P. F. Brevet, H. H. Girault, *J. Chem. Soc.-Faraday Trans.* **91** (1995) 1763–1768.

[50] M. J. Crawford, J. G. Frey, T. J. VanderNoot, Y. G. Zhao, *J. Chem. Soc.-Faraday Trans.* **92** (1996) 1369–1373.

[51] H. F. Wang, E. Borguet, K. B. Eisenthal, *J. Phys. Chem. B* **102** (1998) 4927–4932.

[52] Q. Du, E. Freysz, Y. R. Shen, *Science* **264** (1994) 826–828.

[53] M. C. Messmer, J. C. Conboy, G. L. Richmond, *J. Am. Chem. Soc.* **117** (1995) 8039–8040.

[54] D. E. Gragson, G. L. Richmond, *Langmuir* **13** (1997) 4804–4806.

[55] P. B. Miranda, Y. R. Shen, *J. Phys. Chem. B* **103** (1999) 3292–3307.

[56] L. F. Scatena, M. G. Brown, G. L. Richmond, *Science* **292** (2001) 908–912.

[57] G. L. Richmond, *Annu. Rev. Phys. Chem.* **52** (2001) 357–389.

[58] L. F. Scatena, G. L. Richmond, *J. Phys. Chem. B* **105** (2001) 11240–11250.

[59] J. Strutwolf, A. L. Barker, M. Gonsalves, D. J. Caruana, P. R. Unwin, D. E. Williams, J. R. P. Webster, *J. Electroanal. Chem.* **483** (2000) 163–173.

[60] D. M. Mitrinovic, Z. Zhang, S. M. Williams, Z. Huang, M. L. Schlossman, *J. Phys. Chem. B* **103** (1999) 1779–1782.

[61] D. M. Mitrinovic, A. M. Tikhonov, M. Li, Z. Q. Huang, M. L. Schlossman, *Phys. Rev. Lett.* **85** (2000) 582–585.

[62] A. M. Tikhonov, D. M. Mitrinovic, M. Li, Z. Q. Huang, M. L. Schlossman, *J. Phys. Chem. B* **104** (2000) 6336–6339.

[63] A. Trojanek, P. Krtil, Z. Samec, *J. Electroanal. Chem.* **517** (2001) 77–84.

[64] Z. H. Zhang, I. Tsuyumoto, S. Takahashi, T. Kitamori, T. Sawada, *J. Phys. Chem. A* **101** (1997) 4163–4166.

[65] Y. Uchiyama, I. Tsuyumoto, T. Kitamori, T. Sawada, *J. Phys. Chem. B* **103** (1999) 4663–4665.

[66] Y. Uchiyama, M. Fujinami, T. Sawada, I. Tsuyumoto, *J. Phys. Chem. B* **104** (2000) 4699–4702.

[67] I. Tsuyumoto, H. Uchikawa, *Anal. Chem.* **73** (2001) 2366–2368.

[68] L. X. Dang, *J. Phys. Chem. B* **103** (1999) 8195–8200.

[69] I. Benjamin, *Science* **261** (1993) 1558–1560.

[70] C. J. Slevin, J. V. Macpherson, P. R. Unwin, *J. Phys. Chem. B* **101** (1997) 10851–10859.

[71] A. L. Barker, P. R. Unwin, *J. Phys. Chem. B* **105** (2001) 12019–12031.

[72] C. J. Slevin, P. R. Unwin, *Langmuir* **13** (1997) 4799–4803.

[73] C. J. Slevin, P. R. Unwin, *Langmuir* **15** (1999) 7361–7371.

[74] V. B. Levich, Physicochemical Hydrodynamics, Prentice-Hall, Englewood Cliffs, 1962.

[75] R. Greef, P. R., L. M. Peter, D. Pletcher, J. Robinson, Instrumental Methods in Electrochemistry, Ellis Horwood Ltd., Chichester, 1985.

[76] C. M. A. Brett, A. M. C. F. Oliveira Brett, Hydrodynamic Electrodes, *in:* Comprehensive Chemical Kinetics, C. H. Bamford, R. G. Compton (Eds.), Elseveir, Amsterdam, 1986, Ch. 5, pp. 355–441.

[77] R. G. Compton, P. R. Unwin, *J. Electroanal. Chem.* **205** (1986) 1–20.

[78] A. J. Bard, L. R. Faulkner, Electrochemical Methods: Fundamentals and Applications, John Wiley & Sons, New York, 2001.

[79] J. V. Macpherson, S. Marcar, P. R. Unwin, *Anal. Chem.* **66** (1994) 2175–2179.

[80] J. V. Macpherson, C. E. Jones, P. R. Unwin, *J. Phys. Chem. B* **102** (1998) 9891–9897.

[81] J. V. Macpherson, P. R. Unwin, *Anal. Chem.* **70** (1998) 2914–2921.

[82] J. A. Cooper, R. G. Compton, *Electroanalysis* **10** (1998) 141–155.

[83] J. V. Macpherson, P. R. Unwin, *Anal. Chem.* **71** (1999) 2939–2944.

[84] J. V. Macpherson, *Electroanalysis* **12** (2000) 1001–1011.

[85] J. V. Macpherson, N. Simjee, P. R. Unwin, *Electrochim. Acta* **47** (2001) 29–45.

[86] Z. Samec, V. Mareček, J. Weber, D. Homolka, *J. Electroanal. Chem.* **99** (1979) 385–389.

[87] S. Kihara, M. Suzuki, K. Maeda, K. Ogura, S. Umetani, M. Matsui, Z. Yoshida, *Anal. Chem.* **58** (1986) 2954–2961.

[88] Y. Kubota, H. Katano, K. Maeda, M. Senda, *Electrochim. Acta* **44** (1998) 109–116.

[89] E. Wang, Z. Sun, *Trends Anal. Chem.* **7** (1988) 99–106.

[90] A. Baars, K. Aoki, J. Watanabe, *J. Electroanal. Chem.* **464** (1999) 128–132.

[91] J. Zhang, C. J. Slevin, L. Murtomäki, K. Kontturi, D. E. Williams, P. R. Unwin, *Langmuir* **17** (2001) 821–827.

[92] J. Zhang, C. J. Slevin, P. R. Unwin, *Chem. Commun.* (1999) 1501–1502.

[93] W. J. Albery, J. F. Burke, E. B. Leffler, J. Hadgraft, *J. Chem. Soc., Faraday Trans. 1* **72** (1976) 1618–1626.

[94] J. A. Manzanares, R. Lahtinen, B. Quinn, K. Kontturi, D. J. Schiffrin, *Electrochim. Acta* **44** (1998) 59–71.

[95] V. Mareček, H. Jänchenová, M. P. Colombini, P. Papoff, *J. Electroanal. Chem.* **217** (1987) 213–219.

[96] B. Hundhammer, S. Wilke, *J. Electroanal. Chem.* **266** (1989) 133–141.

[97] S. Wilke, H. Franzke, H. Müller, *Anal. Chim. Acta* **268** (1992) 285–292.

[98] E. Wang, H. Ji, *Electroanalysis* **1** (1989) 75–80.

[99] J. S. Rossier, R. Ferrigno, H. H. Girault, *J. Electroanal. Chem.* **492** (2000) 15–22.

[100] H. J. Lee, C. M. Pereira, A. F. Silva, H. H. Girault, *Anal. Chem.* **72** (2000) 5562–5566.

[101] Q. Fulian, A. C. Fisher, R. A. W. Dryfe, E. P. L. Roberts, *J. Electroanal. Chem.* **483** (2000) 197–200.

[102] K. A. Gooch, N. A. Williams, A. C. Fisher, *Electrochem. Commun.* **2** (2000) 51–55.

[103] C. J. Slevin, P. R. Unwin, Hydrodynamic Techniques for Investigating Reaction Kinetics at Liquid-Liquid Interfaces: Historical Overview and Recent Developments, *in:* Surfactant Science Series, Vol. 95, A. G. Volkov (Ed.), Marcel Dekker, New York, 2001, Ch. 13, pp. 325–353.

[104] T. Singh, J. Dutt, *J. Electroanal. Chem.* **190** (1985) 65–73.

[105] R. G. Compton, M. B. G. Pilkington, G. M. Stearn, P. R. Unwin, *J. Electroanal. Chem.* **238** (1987) 43–66.

[106] H. H. J. Girault, D. J. Schiffrin, *J. Electroanal. Chem.* **179** (1984) 277–284.

[107] T. Kakiuchi, M. Yamane, T. Osakai, M. Senda, *Bull. Chem. Soc. Jpn.* **60** (1987) 4223–4228.

[108] T. Kakiuchi, M. Kobayashi, M. Senda, *Bull. Chem. Soc. Jpn.* **61** (1988) 1545–1550.

[109] T. Kakiuchi, M. Nakanishi, M. Senda, *Bull. Chem. Soc. Jpn.* **61** (1988) 1845–1851.

[110] T. Kakiuchi, M. Nakanishi, M. Senda, *Bull. Chem. Soc. Jpn.* **62** (1989) 403–409.

[111] J. Koryta, L. Q. Hung, A. Hofmanova, *Stud Biophys* **90** (1982) 25–29.

[112] V. J. Cunnane, D. J. Schiffrin, M. Fleischmann, G. Geblewicz, D. Williams, *J. Electroanal. Chem.* **243** (1988) 455–464.

[113] T. Kakiuchi, M. Kotani, J. Noguchi, M. Nakanishi, M. Senda, *J. Colloid Interface Sci.* **149** (1992) 279–289.

[114] T. Kakiuchi, T. Kondo, M. Kotani, M. Senda, *Langmuir* **8** (1992) 169–175.

[115] A.-K. Kontturi, K. Kontturi, L. Murtomäki, B. Quinn, V. J. Cunnane, *J. Electroanal. Chem.* **424** (1997) 69–74.

[116] T. Kakiuchi, T. Kondo, M. Senda, *Bull. Chem. Soc. Jpn.* **63** (1990) 3270–3276.

[117] B. Quinn, K. Kontturi, *J. Electroanal. Chem.* **483** (2000) 124–134.

[118] M. H. Delville, M. Tsionsky, A. J. Bard, *Langmuir* **14** (1998) 2774–2779.

[119] M. Tsionsky, A. J. Bard, M. V. Mirkin, *J. Am. Chem. Soc.* **119** (1997) 10785–10792.

[120] J. Zhang, P. R. Unwin, *J. Electroanal. Chem.* **494** (2000) 47–52.

[121] D. G. Georganopoulou, J. Strutwolf, C. M. Pereira, F. Silva, P. R. Unwin, D. E. Williams, *Langmuir* **17** (2001) 8348–8354.

[122] J. Strutwolf, J. Zhang, A. L. Barker, P. R. Unwin, *Phys. Chem. Chem. Phys.* **3** (2001) 5553–5558.

[123] J. Zhang, P. R. Unwin, *Langmuir* **18** (2002) 2313–2318.

[124] D. Grandell, L. Murtomäki, *Langmuir* **14** (1998) 556–559.

[125] D. Grandell, L. Murtomäki, K. Kontturi, G. Sundholm, *J. Electroanal. Chem.* **463** (1999) 242–247.

[126] D. Grandell, L. Murtomäki, G. Sundholm, *J. Electroanal. Chem.* **469** (1999) 72–78.

[127] D. G. Georganopoulou, D. J. Caruana, J. Strutwolf, D. E. Williams, *Faraday Discuss.* (2000) 109–118.

[128] R. A. W. Dryfe, S. M. Holmes, *J. Electroanal. Chem.* **483** (2000) 144–149.

[129] G. C. Lillie, R. A. W. Dryfe, S. M. Holmes, *Analyst* **126** (2001) 1857–1860.

[130] R. A. W. Dryfe, B. Kralj, *Electrochem. Commun.* **1** (1999) 128–130.

[131] B. Kralj, R. A. W. Dryfe, *Phys. Chem. Chem. Phys.* **3** (2001) 5274–5282.

[132] R. A. W. Dryfe, S. M. Holmes, B. Krajl, G. C. Lillie , Nano–templated electrode surfaces, oral presentation at Electrochem2001, Loughborough University, 2001.

[133] Y. Cheng, R. M. Corn, *J. Phys. Chem. B* **103** (1999) 8726–8731.

[134] Y. Cheng, L. Murtomäki, R. M. Corn, *J. Electroanal. Chem.* **483** (2000) 88–94.

[135] A. Mälkiä, P. Liljeroth, K. Kontturi, *Anal. Sci.* **17** (2001) i345–i348.

[136] A. J. Bard, F.-R. F. Fan, M. V. Mirkin, Scanning Electrochemical Microscopy, *in:* Electroanalytical Chemistry, Vol. 18, A. J. Bard (Ed.), Marcel Dekker, New York, 1994, pp. 244–392.

[137] P. R. Unwin, *J. Chem. Soc.-Faraday Trans.* **94** (1998) 3183–3195.

[138] M. V. Mirkin, *Anal. Chem.* **68** (1996) A177–A182.

[139] M. V. Mirkin, *Mikrochim. Acta* **130** (1999) 127–153.

[140] M. V. Mirkin, B. R. Horrocks, *Anal. Chim. Acta* **406** (2000) 119–146.

[141] G. Nagy, L. Nagy, *Fresenius J. Anal. Chem.* **366** (2000) 735–744.

[142] A. J. Bard, F. R. F. Fan, J. Kwak, O. Lev, *Anal. Chem.* **61** (1989) 132–138.

[143] A. J. Bard, F. R. F. Fan, D. T. Pierce, P. R. Unwin, D. O. Wipf, F. M. Zhou, *Science* **254** (1991) 68–74.

[144] A. J. Bard, D. E. Cliffel, C. Demaille, F. R. F. Fan, M. Tsionsky, *Ann. Chim.* **87** (1997) 15–31.

[145] C. J. Slevin, J. Zhang, P. R. Unwin, *J. Phys. Chem. B* **106** (2002) 3019–3025.

[146] G. Zhao, D. M. Giolando, J. R. Kirchoff, *Anal. Chem.* **67** (1995) 1491–1495.

[147] Y. Lee, S. Amemiya, A. J. Bard, *Anal. Chem.* **73** (2001) 2261–2267.

[148] J. Ufheil, K. Borgwarth, J. Heinze, *Anal. Chem.* **74** (2002) 1316–1321.

[149] Z. Ding, Ph. D. Thesis, Departement de Chimie, Swiss Federal Institute of Technology in Lausanne (EPFL), Lausanne, 1999.

[150] V. J. Cunnane, G. Geblewicz, D. J. Schiffrin, *Electrochim. Acta* **40** (1995) 3005–3014.

[151] J. Kwak, A. J. Bard, *Anal. Chem.* **61** (1989) 1221–1227.

[152] Q. Fulian, A. C. Fisher, G. Denuault, *J. Phys. Chem. B* **103** (1999) 4387–4392.

[153] Q. Fulian, A. C. Fisher, G. Denuault, *J. Phys. Chem. B* **103** (1999) 4393–4398.

[154] J. L. Amphlett, G. Denuault, *J. Phys. Chem. B* **102** (1998) 9946–9951.

[155] Y. Selzer, D. Mandler, *Anal. Chem.* **72** (2000) 2383–2390.

[156] A. J. Bard, M. V. Mirkin, P. R. Unwin, D. O. Wipf, *J. Phys. Chem.* **96** (1992) 1861–1868.

[157] P. R. Unwin, A. J. Bard, *J. Phys. Chem.* **95** (1991) 7814–7824.

[158] R. D. Martin, P. R. Unwin, *Anal. Chem.* **70** (1998) 276–284.

[159] R. D. Martin, P. R. Unwin, *J. Chem. Soc.-Faraday Trans.* **94** (1998) 753–759.

[160] R. D. Martin, P. R. Unwin, *J. Electroanal. Chem.* **439** (1997) 123–136.

[161] A. L. Barker, P. R. Unwin, S. Amemiya, J. F. Zhou, A. J. Bard, *J. Phys. Chem. B* **103** (1999) 7260–7269.

[162] A. L. Barker, J. V. Macpherson, C. J. Slevin, P. R. Unwin, *J. Phys. Chem. B* **102** (1998) 1586–1598.

[163] A. L. Barker, P. R. Unwin, J. Zhang, *Electrochem. Commun.* **3** (2001) 372–378.

[164] C. J. Slevin, P. R. Unwin, *J. Am. Chem. Soc.* **122** (2000) 2597–2602.

[165] J. Zhang, C. J. Slevin, C. Morton, P. Scott, D. J. Walton, P. R. Unwin, *J. Phys. Chem. B* **105** (2001) 11120–11130.

[166] J. Zhang, P. R. Unwin, *J. Am. Chem. Soc.* **124** (2002) 2379–2383.

[167] A. J. Bard, G. Denault, R. A. Friesner, B. C. Dornblaser, L. S. Tuckerman, *Anal. Chem.* **63** (1991) 1282–1288.

[168] D. J. Gavaghan, *J. Electroanal. Chem.* **456** (1998) 1–12.

[169] J. Galceran, J. Cecilia, E. Companys, J. Salvador, J. Puy, *J. Phys. Chem. B* **104** (2000) 7993–8000.

[170] D. J. Gavaghan, *J. Electroanal. Chem.* **456** (1998) 13–23.

[171] D. J. Gavaghan, *J. Electroanal. Chem.* **456** (1998) 25–35.

[172] J. Heinze, *J. Electroanal. Chem.* **124** (1981) 73–86.

[173] J. Heinze, M. Storzbach, *Ber. Bunsen-Ges.* **90** (1986) 1043–1048.

[174] G. Taylor, H. H. Girault, J. McAleer, *J. Electroanal. Chem.* **293** (1990) 19–44.

[175] K. Aoki, J. Osteryoung, *J. Electroanal. Chem.* **160** (1984) 335–339.

[176] D. Shoup, A. Szabo, *J. Electroanal. Chem.* **140** (1982) 237–245.

[177] A. Szabo, *J. Phys. Chem.* **91** (1987) 3108–3111.

[178] K. B. Oldham, *J. Electroanal. Chem.* **122** (1981) 1–17.

[179] J. C. Myland, K. B. Oldham, *J. Electroanal. Chem.* **153** (1983) 43–54.

[180] D. K. Cope, C. H. Scott, D. E. Tallman, *J. Electroanal. Chem.* **285** (1990) 49–69.

[181] B. A. Brookes, D. J. Gavaghan, R. G. Compton, *J. Phys. Chem. B* **106** (2002) 4886–4896.

[182] M. V. Mirkin, F. R. F. Fan, A. J. Bard, *J. Electroanal. Chem.* **328** (1992) 47–62.